Physiological Analyses of Broadband Near-Infrared Spectroscopy and Electrophysiological Measurements in vivo for Biomedical Applications

by

Haylea Renguul

THESIS

Presented to the Faculty of the Graduate School of

The University of Texas at Arlington in Partial Fulfillment

of the Requirements

For the Degree of

MASTER OF SCIENCE IN BIOMEDICAL ENGINEERING

THE UNIVERSITY OF TEXAS AT ARLINGTON

MAY 2023

Acknowledgements

I would like to thank Dr. Hanli Liu for her guidance and mentorship throughout my master's degree. Her knowledge, advice, and support have helped me immeasurably during my studies and the process of writing this thesis. I am also grateful to my defense committee members, Dr. Alexandrakis and Dr. Ortigoza. In particular, I'd like to thank Dr. Ortigoza for his counsel in interpretation and discussion for the Electrogastrography (EGG) project.

Additionally, I wish to express my gratitude to all of my past and present lab colleagues for their support and collaboration during my studies. I greatly appreciate Abhilash Boppana, Elizabeth Rhodes, and Soheila Norasteh for their assistance with the analysis of EGG data. I also thank Caroline Carter, Claire Sissons, and Dr. Matthew Brothers' lab for data collection during our occlusion test measurements. My thanks also go to Dr. Sadra Shahdadian for teaching me many different data processing and analysis techniques.

Finally, I'd like to thank my friends and family for all of their love and support during my journey. I'm especially grateful to my parents for their endless belief in me – for I'm just as endlessly inspired by them.

Table of Contents

List of Figures

List of Tables

Abstract

Physiological Analyses of Broadband NIRS and Electrophysiological Measurements in vivo for Biomedical Applications

Haylea Renguul

The University of Texas at Arlington, 2023

Supervising Professor: Dr. Hanli Liu

My thesis concerns analysis of data from optical and electrophysiological measurement tools for calculate potential biomarkers in three biomedical applications: (1) the gastrointestinal immaturity of infants of different ages, (2) prefrontal connectivity in healthy older adults, and (3) hemodynamic-metabolic coherence during vascular occlusion. The first application relied on electrogastrogram (EGG) measurements taken on 81 newborns in a neonatal intensive care unit. Of the 81 babies, 77 were born prematurely. By separating these babies into different gestational age groups and analyzing their EGG data, I was able to find population differences in common EGG analysis parameters. In particular, we found that the mean power ratio between the during- and pre-feeding periods increased as the gestational age of infants increased. Similarly, the full-term (i.e. born at 37 weeks of pregnancy or later) babies consistently showed higher power ratios when comparing the post- and pre-feeding periods. These results imply that power ratio is a robust parameter to use when measuring gastrointestinal maturity in both infants and adults.

The second biomedical application regarded prefrontal connectivity in healthy older adults by analyzing infra-slow oscillation (ISO) waves. This area is a pressing topic, as lower rates of prefrontal connectivity have been associated with Alzheimer's Disease (AD), which affects nearly 10% of older adults. The current study also followed-up on a previous study from

our lab, in which the ISO waves of healthy younger adults were analyzed to assess prefrontal connectivity. That study established a range of values for multiple ISO-derived parameters, including spectral amplitude and connectivity. I found that the results from older adults were largely in the same ranges, except for spectral amplitude in the myogenic band and unilateral coupling across all ISO bands. This suggests that older adults may have lower myogenic responses due to the stiffening of the vascular wall with age, and that unilateral coupling of oxygenated hemodynamics and metabolism may actually increase with age. However, the sample size was limited to six subjects, so future measurements are needed to better establish the ranges for ISO-derived parameters in older adults.

Lastly, the third biomedical application was to study the robustness of Wavelet Transform Coherence (WTC) in analyzing Near-Infrared Spectroscopy (NIRS) data taken during a vascular occlusion test. Vascular occlusion tests are usually performed in clinical settings to measure blood pressure. However, these tests are also useful for testing tools like NIRS, with which biological signals like oxygenated hemoglobin (HbO) and cytochrome C oxidase (CCO; an enzyme coupled with metabolic rate) can be measured. My lab-mates recorded NIRS data on seven subjects within our lab while conducting a vascular occlusion test. I then analyzed the data using WTC, which is a time-frequency analysis tool that has yet to be applied to HbO and CCO. This resulted in heat maps for each subject, within which we could analyze different the power of different ISO bands during occlusion. This study illustrates how HbO and CCO mediate the supply-and-demand relationship between oxygen and blood when the oxygen supply is starved.

CHAPTER 1

Analysis of Electrogastrography to Evaluate Gastral Health of Newborns

1.1 Introduction

1.1.1 Gastrointestinal Health of Newborns

Gastrointestinal immaturity, or the underdevelopment of one's digestive system, is linked to necrotizing enterocolitis (NEC), which is an illness that causes cellular damage and death to in the colon and intestine (1). NEC has a mortality rate of 50% and is one of the leading causes of death in preterm babies. However, the symptoms of NEC vary widely and can go undetected by parents; common measures of NEC are often relative measures, such as feeding intolerance, blood in stool, and an increase in abdominal girth (2). Consequently, there is a need to establish objective biomarkers of NEC so that diagnosis and treatment can begin soon after the illness takes root. The gastrointestinal immaturity of premature infants is widely understood to be correlated with gestational age, which is the amount of time between the first day of a mother's last menstrual cycle to the date of her child's birth. The second and third trimesters are particularly crucial in digestive tract development (3, 4). Thus, a baby's digestive system is considered to be fully developed the 37^{th} week and older. However, there are very few published findings regarding the correlation of a baby's gestational age, or the time when the baby stays in his/her mother's womb, and the gastrointestinal maturity. Therefore, there is a need for a non-invasive method of observing gastrointestinal development after early birth of preterm neonates.

1.1.2 Electrogastrography

An understudied tool that lends itself to my first topic is electrogastrography (EGG). EGG is a non-invasive tool that records contractions of the gastrointestinal tract using cutaneous electrodes

on a subject's abdomen. The resulting electrogastrogram is a multi-channel recording of voltage over time. These voltage signals can be processed and analyzed using standard signal processing techniques to determine if a subject exhibits normal or abnormal gastric patterns. There are three gastric frequency bands that are observed in EGG: bradygastria (0.5 – 2 cycles per minute (cpm)), normogastria (2 – 4 cpm), and tachygastria (4 – 9 cpm). The normogastria band is associated with healthy gastric motility and is centered around 3 cpm, which is the frequency at which stomach activity peaks. This 3 cpm peak is a common characteristic of EGG in adults. Conversely, bradygastria and tachygastria are associated with abnormal digestive behavior, such as nausea, indigestion, and delayed gastric emptying. Consequently, the power of EGG signals in these frequency bands can indicate the health of a subject's gastrointestinal tract. Although the first EGG was established in 1921, the tool has gained widespread usage only in the last three decades (5). Thus, its application and usage have mostly been limited to adult populations. There are very few published studies about the usage of EGG on infants, and there are even fewer studies about its application on premature infants. Since EGG can provide quantitative insights into gastric motility, it can potentially mark gastrointestinal immaturity in premature infants and, consequently, objective signs of NEC. In this study, I seek to establish EGG biomarkers of premature babies of a variety of gestational ages to set the stage for future comparisons with babies diagnosed with NEC.

1.1.3 Previous Studies on Electrogastrography Applications in Newborns

Previous studies on the spectral analysis of EGG generally calculated several parameters, such as: mean power spectral density (mPSD), dominant frequency and power of EGG signal, and power ratio of EGG between fasting and post-feeding periods. These parameters are very useful for characterizing EGG patterns, and we have used similar approaches to two of them in

our study. However, the primary method for frequency analysis of EGG has remained relatively unchanged and unchallenged for decades. The first publications on EGG power spectra were predicated on the results of a single Fast Fourier Transform (FFT), but more recent publications utilize a form of Running Spectral Analysis (RSA) with a Hamming window. Both of these techniques have room to be streamlined. In my study, we have deployed the commonly-used Welch's method, whose overlapping-window factor allows for more noise reduction and less information loss in comparison with other methods. Welch's method also takes less time to generate spectra, allowing us to have a much higher through-put of power spectra.

There are also shortcomings with the experimental setup of previous studies regarding EGG. In the past, only the pre-feeding and post-feeding periods were recorded using EGG. This leaves little to no information about the activity of the gastrointestinal tract during-feeding, a period that could reveal significant information about gut motility during digestion. Additionally, previous studies tended towards smaller population sizes, with many of them only including up to twenty neonatal subjects. The small population sizes further inhibited longitudinal recordings or multiple weekly recordings over the course of hospital stays. In our study, the data that was analyzed includes multiple (ten or more) weeks of EGG recordings taken from Parkland Hospital, which allows for longitudinal analysis. Lastly, we have separated our premature neonates into two distinct categories: early-term (infants born at less than 29 weeks of gestation) and mid-term (infants born at 29 – 33 weeks). This distinction, alongside several fully developed term infants, allows us to conduct a group-level analysis of EGG-derived metrics between different gestational age ranges. Therefore, the current study has sought to further illuminate the gastric motility of premature babies along different gestational ages.

More recently, a study published by Chaudhari et. al. in 2022 proposed a novel methodology to analyze and characterize PSD in EGG, which is more efficient than, but still as precise as, past methods (7). The study also analyzed PSD in during-feeding periods. My current study employs this new methodology but updates its application by looking at PSD dependence on both gestational age and longitudinal postmenstrual age (PMA) in preterm babies. I also included 33 more subjects in my analysis. Although the paper from Chaudhari et. al. is novel and provides the foundation for the current study, it was limited by assuming that the average of all recorded weeks of a newborn were representative of his/her gastric health at birth. That is, there was no consideration of the progressive changes in PSD as the postmenstrual age of each subject increased. I have also expanded upon Dr. Chaudhari's data analysis by including the power ratio parameter, which allows quantification of power changes in each frequency band during and after feeding is completed. The advantage of this power ratio approach is its excellent ability of self-calibration for each baby to remove uncertainty caused by device setup, recording times and conditions, and individual variability. Accordingly, one of the novel goals of this study was to characterize PSD features in preterm infants over time.

1.1.4 Goals of This Study

The objectives of this study were as follows:

(1) Investigate potential biomarkers for mPSD and power ratio in all three frequency bands (bradygastria, normogastria, and tachygastria) in three age ranges of infants (early-term babies, mid-term babies, and full-term babies) during all three periods (pre-feeding, during-feeding, and post-feeding) in their earliest recorded week of life.

(2) Investigate possible linearity between mPSD and gestational age to signify a baby's gut development during pregnancy.

(3) Analyze patterns in power spectra curves at a group-level and compare them with EGG characteristics in healthy adults, particularly 3 cpm normogastric peaks.

(4) Observe longitudinal changes in mPSD and power ratio as infants age.

1.2 Methodology

1.2.1 Study Design

From 2017-2020, Parkland Health and Hospital System and Children's Health (Dallas, TX) recorded data from eighty-one neonates (77 premature and 4 full-term) after obtaining parental consent. The Institutional Review Board at The University of Texas Southwestern Medical Center approved this study. Participants were separated into two primary categories, premature (neonates born at less than 34 weeks of gestational age (GA)) and term (neonates born at 37 or more weeks of GA). The premature neonates were further split into two subcategories: early (younger than 29 weeks of GA) and mid (29-33 weeks of GA). Infants with known congenital or chromosomal disorders, significant medical instability, and/or significant skin abnormalities were excluded from the study. Once a week, both EGG and NIRS signals were recorded. These weekly recordings continued until the participant reached a full-term PMA (37 weeks), passed away, or were withdrawn from the study by their parents and/or medical team.

1.2.2 Experimental Setup

1.2.2.1 Electrogastrography (EGG)

The EGG setup consisted of three channels, whose electrode placement is shown in Figure 1. This electrode placement concurs with the method presented by Chen et al. EGG data was acquired using a BIOPAC® MP36 acquisition unit (BIOPAC Systems, Inc., Goleta, CA), with a sampling rate of 2000 Hz (6).

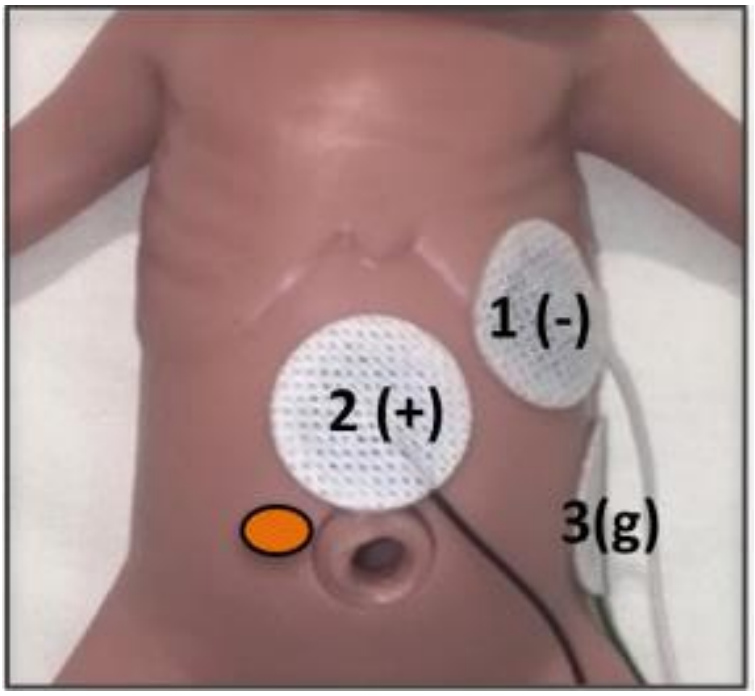

Figure 1-1: The setup of the three EGG electrodes. “1 (-)” marks the negative electrode, “2 (+)” marks the positive electrode, and “3 (g)” marks the ground electrode. The orange oblong notes the abdominal Near-Infrared Spectroscopy sensor. Sourced from Chaudhari et. al.

1.2.2.2 Near-Infrared Spectroscopy (NIRS)

Two Neonatal INVOS^{TM} Infant Regional Saturation Sensors (Covidient Ltd., Minneapolis, MN) were used in this study. One was placed on the abdomen (as shown in Figure 1-1) and the other was placed on the forehead. These sensors measured abdominal optical density and cerebral optical density, respectively. A Vital Sync^{TM} 5000 System (Covidient Ltd., Minneapolis, MN) synchronized concurrent recordings from a cardiorespiratory monitor and the INVOS system. Neither of the NIRS signals were considered in the current study, as my goals were to characterize and analyze EGG signals, but they have been preserved in order to be included in future analysis.

1.2.2.3 Feeding

Infants were fed using an enteral feeding tube, as shown in Figure 1-2. The timing of feedings was determined by Parkland's neonatal intensive care unit (NICU); however, most of the infants were fed every three hours. Consequently, EGG recordings were at least six hours to include two pre- feeding, two feeding, and two post- feeding periods. In particular, we included subjects with at least thirty minutes of data in each of these six periods. The processing and analysis of these recordings are described in the subsequent sections.

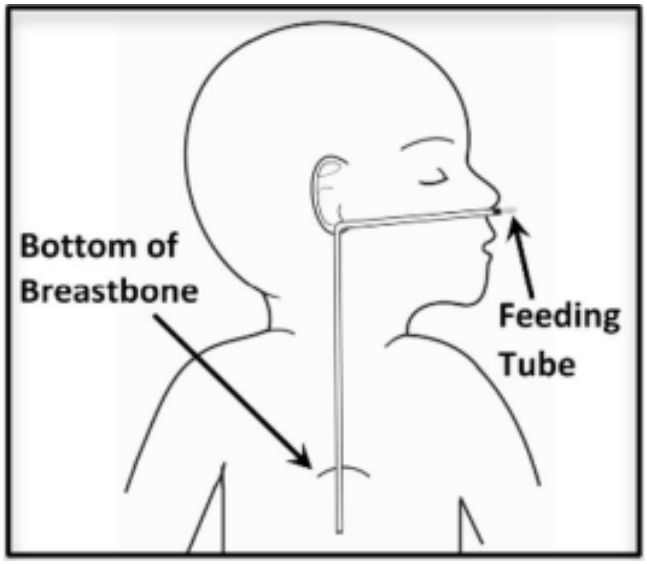

Figure 1-2: An illustration of the setup for enteral feeding. Sourced from Chaudhari et. al.

1.2.3 Data Processing

The flowchart describing the data processing procedure is shown below in figure 1-3.

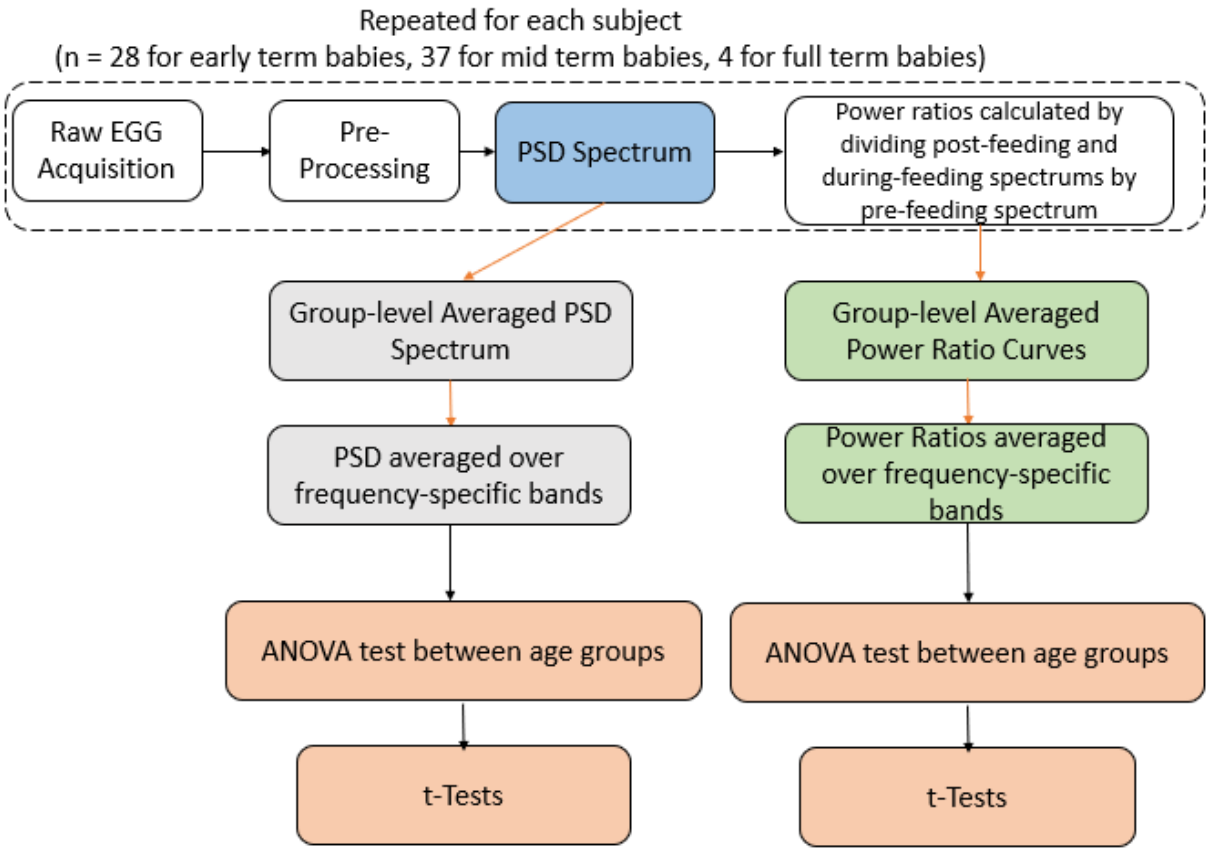

Figure 1-3: Flowchart for data processing steps. The t-tests were Bonferroni-corrected.

1.2.3.1 Pre-Processing

The EGG data was collected with a sampling rate of 2000 Hz. All data processing was conducted in MATLAB using the signal processing toolbox. EGG data pre-processing involved the following steps: (1) down-sampling data to 500 Hz using "downsample"; (2) de-trending by subtracting the third-polynomial fitted line (obtained from "polyfit") from the down-sampled temporal data; (3) zero-phase low-pass filtering on the de-trended data with a cutoff frequency of 1 Hz using "filtfilt".

Additionally, in order to determine if outlier removal was necessary for the raw EGG time series data, we applied the Hampel removal method to a single subject's data. The Hampel

filter is a variation of the three-sigma rule of statistics, and it was chosen due to its robustness against outliers. The results of the Hampel filter as applied to are shown in figure 1-4. The only outliers that the method flagged were local maxima, which were consequently left in the filtered output since the Hampel method will not remove local maxima. Subsequently, we decided not to use a Hampel filter on the raw time-series data.

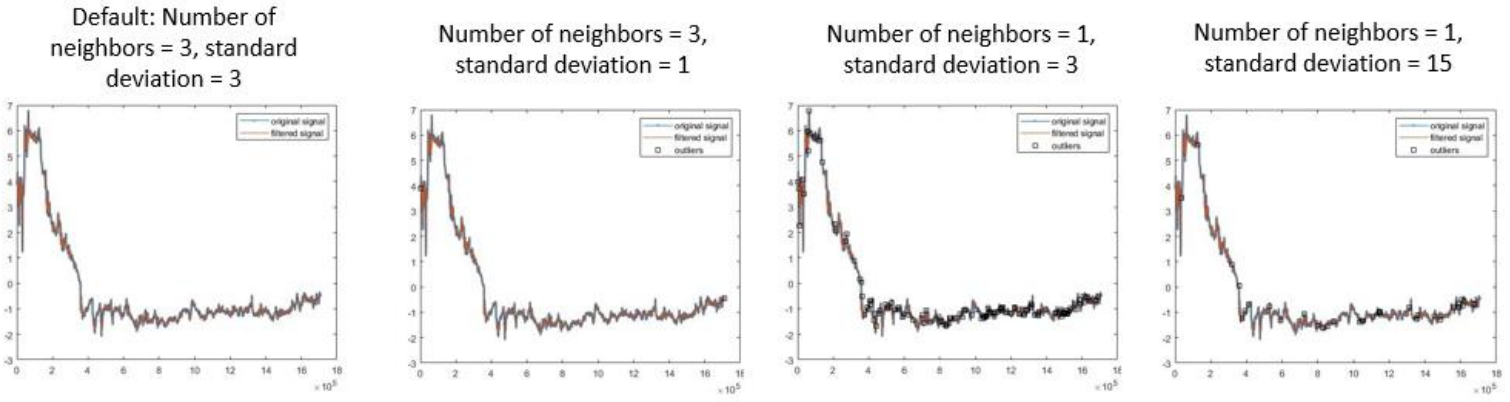

Figure 1-4: The results of the Hampel removal method plotted alongside the original time-series data.

Similarly, we tested the usage of a Hanning window on the time-series data before inputting it to the "pwelch" function. To this, we used a sample of 10 random early-term babies and averaged the results together. We compared two window sizes: 4 minutes, which is the window size that we've chosen to use for the EGG data, and 1 minute. The results are shown in figure 1-5 below, alongside the result from using no Hanning window. The most spectral resolution was achieved in the method with no Hanning window, likely caused by the Hanning window smoothing the signal before it was further smoothed by Welch's method. As a result, we've chosen to not apply a window function to the data before calculating PSD.

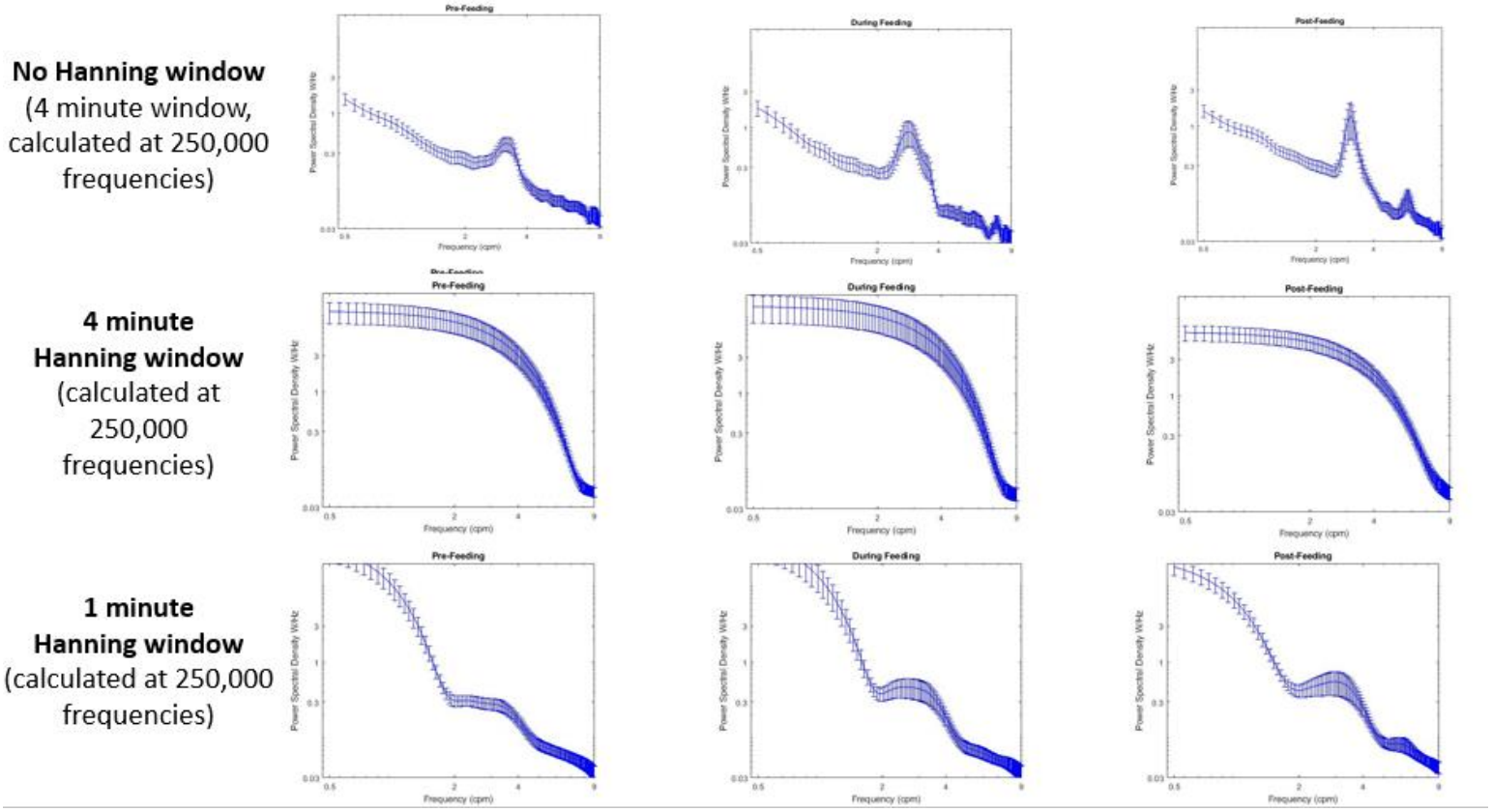

Figure 1-5: The results from an average PSD for 10 early-term babies using different Hanning window sizes.

1.2.3.2 Feeding Period Selection

Each recording was split into six periods, with two periods of pre-feeding, during-feeding, and post-feeding. In our analysis, we solely processed recordings with at least 30 minutes of data in each of these sub-periods. To ensure uniformity, only the first 30 minutes of these sub-periods was included in analysis.

1.2.3.3 Power Spectral Density Calculation

Power Spectral Density (PSD) provides quantitative insight into the intensity of EGG in different frequency bands. In this study, PSD was calculated with Welch's method by using the function "pwelch". A window size of four minutes was chosen, with an overlap of 50% between windows and a 500,000-point Discrete Fourier Transform applied to each window. Some subjects were not recorded during their birth week or had less than 30 minutes of data in their sub-periods during their birth week recording. Consequently, the PSD for every *available* week of a subject was calculated. Group-level averages were taken for early, mid, and term subjects, respectively, in their first available week to generate a plot of the average PSD curve for each age group.

Additionally, the mean PSD (mPSD) was calculated as a parameter for analysis in each frequency band. The values of the PSD curve were averaged to a singular value in each band for each group and sub-period, as well as for individual subjects. For example, the bradygastria mPSD for early subjects would refer to the average value of the PSD curve for early subjects (in Figure 1-6) from 0.5 – 2 cpm. The mPSD values for each subject was also used to generate a linear regression plot for mPSD versus GA, as shown in Figure 1-8.

The mPSD value can illuminate the most prominent gut behaviors for a subject. A large normogastria mPSD value suggests healthy, normal gut behavior, while a large bradygastria or tachygastria mPSD value can indicate indigestion and feeding intolerance. Therefore, in our method, the ideal healthy subject would have a comparatively low mPSD in bradygastria and tachygastria and a higher mPSD in normogastria. The group-level mPSD can also elucidate the average stage of gut development that our premature subjects were in.

1.2.3.4 Power Ratio Calculation

In this study, the pre-prandial period was considered as the baseline for each subject. With this baseline, two power ratios curves were calculated using the PSD for each subject: during-feeding divided by pre-feeding, and post-feeding divided by pre-feeding. After the calculation of power ratio curves, subjects were then separated into the three GA groups, wherein their curves were averaged to obtain group-level power ratio curves. Additionally, the mean power ratio (mPR) in each frequency band was calculated by averaging the values of the power ratio curve in each band for each subject. Since two conditions were considered in the power ratio calculation (during-feeding and post-feeding), there were two mPR values in each frequency band.

The power ratio parameter is useful because it is a self-normalizing factor, which removes some of the noise that arises in comparisons between subjects, and because it is a recurrent parameter in EGG studies. Power ratio is often calculated alongside dominant frequency as a characteristic of EGG analysis. An additional novelty in our study is the calculation of power ratio for the during-feeding period, as power ratio has historically referred to the ratio of the post-feeding spectrum to the pre-feeding spectrum. By looking at two power ratios, we are able to determine how much the GI tract is altered by feeding intervention. In particular, a power ratio larger than one is considered to be a marker of healthy gastric motility.

1.3 Results

1.3.1 Study Cohort

The study included 88 subjects, 81 of which were used for analysis. Seven subjects were excluded due to a lack of noted feeding times, or for having sub-feeding periods that were less than 30 minutes. Of the 81 subjects, nine eventually received a feeding intolerance diagnosis. Six subjects developed feeding intolerance, three subjects were categorized with pathological feeding intolerance. Five of the 81 subjects died during the course of the study.

1.3.2 Average Power Spectra Curves for Age Groups

Figures 1-6 and 1-7 show the average power spectra for each of the GA groups. To maintain consistency over what subjects were considered in the early-term and mid-term categories, only the first week (or the second week, if the first was unavailable) was used in this analysis. Figure 1-6 averages these first and second weeks by GA group, while figure 1-7 only shows the average curves for subjects in their birth week. In figure 1-6, the early-term subjects show the distinct 3 cpm peak that is characteristic of healthy stomach activity. Similarly, in figure 1-7, the early-term subjects most notably display this peak in the post-feeding period. The other GA groups do not show this 3 cpm peak.

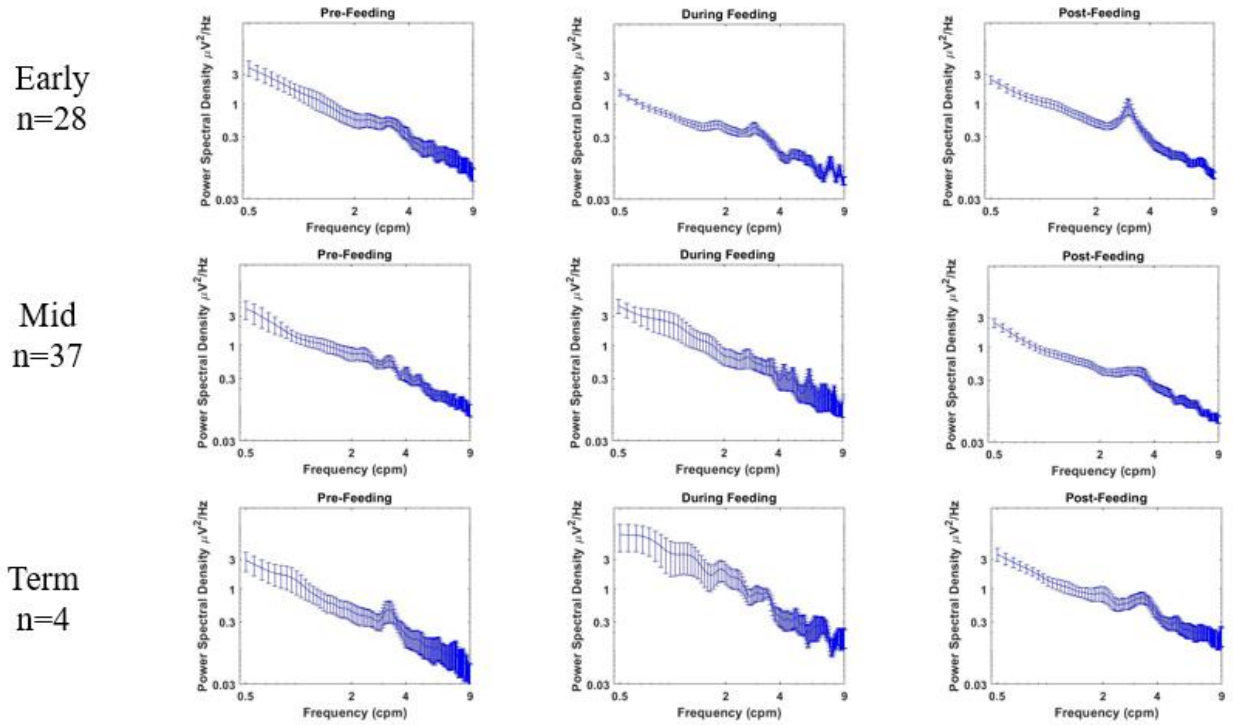

Figure 1-6: The average power spectra curves for all GA groups. The first column notes the pre-feeding period, the second column marks the during-feeding period, and the third column marks the post-feeding period. The rows correspond to each age group. Each spectra averages the first available week for each subject.

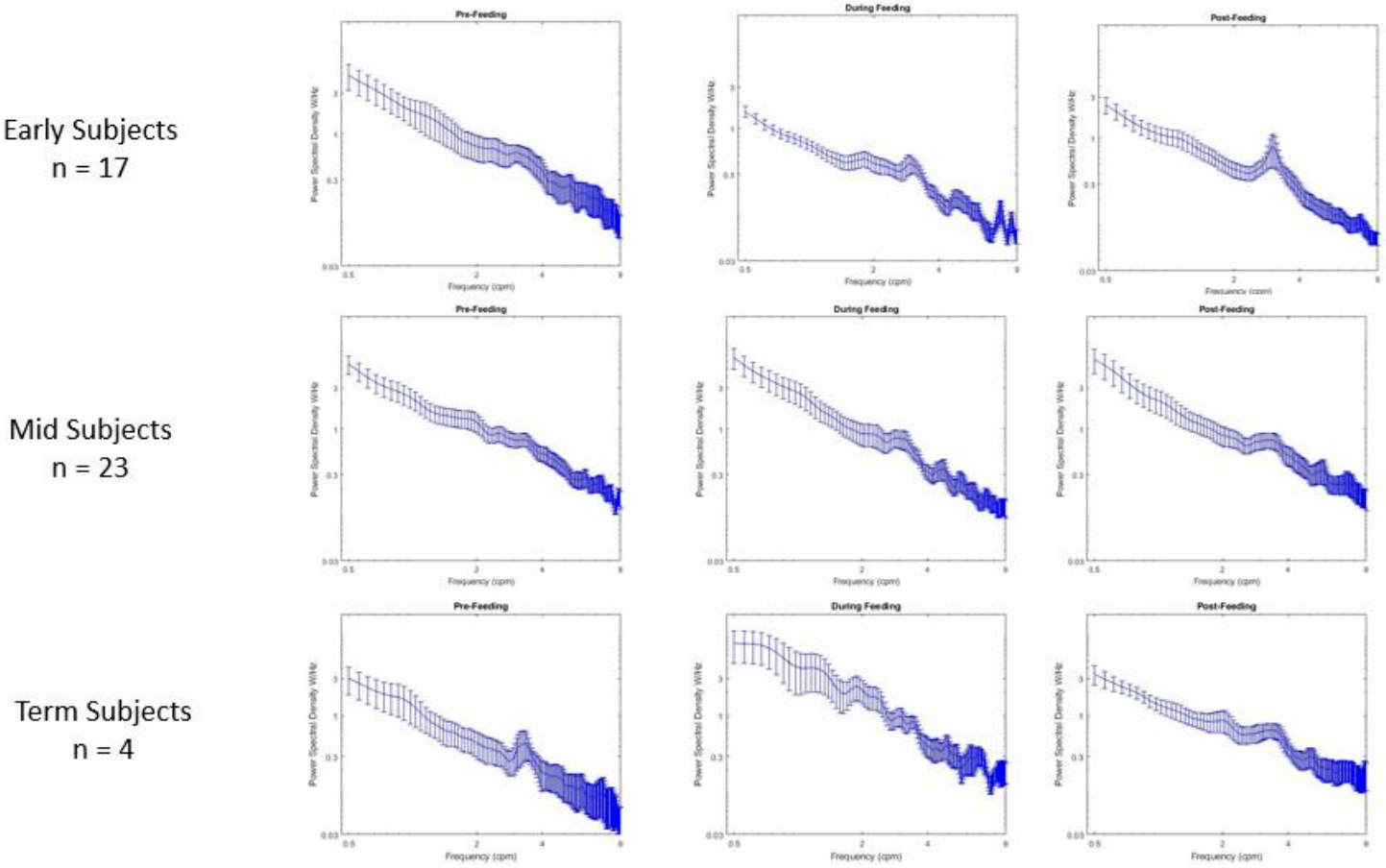

Figure 1-7: The average power spectra curves for subjects in their birth week (i.e. at their gestational age). The columns and rows follow the order of figure 1-6 above.

1.3.3 Mean PSD Comparison Between the Gestational Age Groups

After calculating mPSD values in each frequency band and time period for each subject, nine linear regressions were calculated to compare mPSD versus gestational age. Three outlier subjects were removed from the mid-term group. The results of these regressions are shown in figure 1-8. The bradygastria band in the during-feeding period is the only linear regression that shows a significant increase in mPSD along gestational age. Although the sample size for term babies is very small, it can serve as a reference point for a range of mPSD values for full-term neonates.

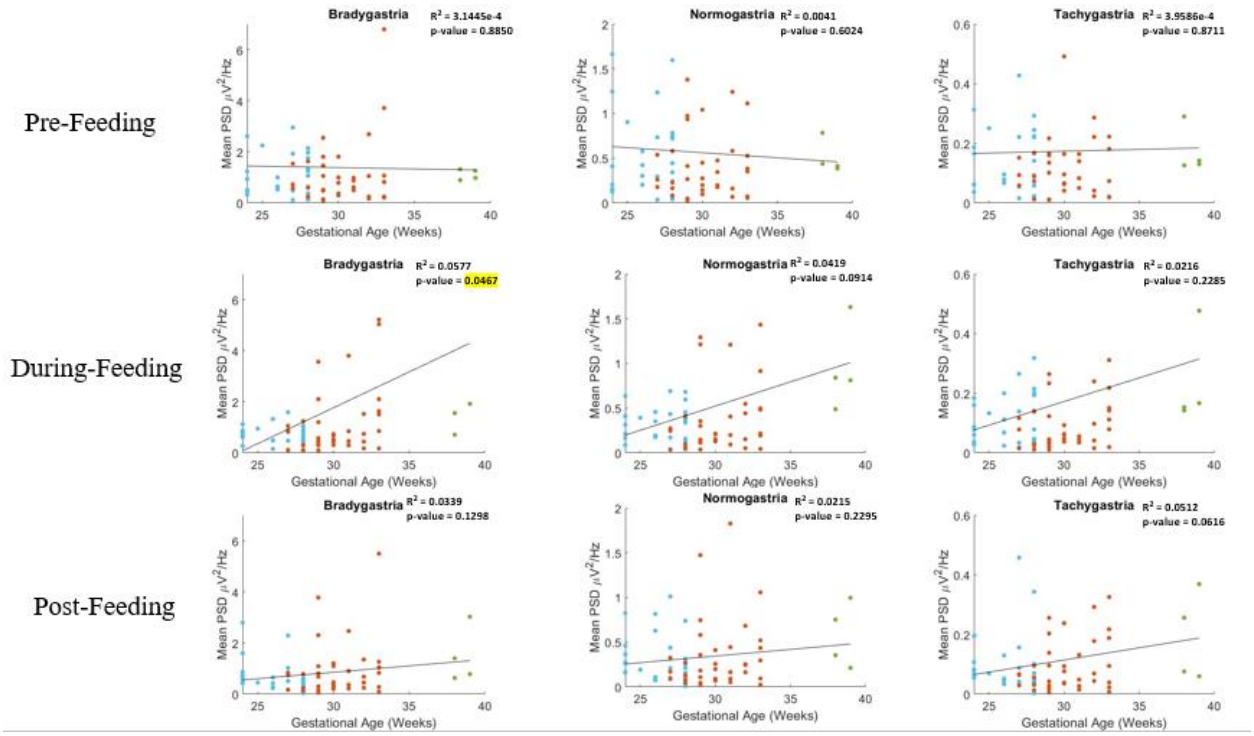

Figure 1-8: Linear regression for the mean PSD versus the gestational age of subjects. There are 32 early-term babies (blue), 45 mid-term babies (red), and 4 full-term babies (green) included in these plots. The columns showcase the three frequency bands, and the rows indicate the feeding periods. p-values and ordinary R^2 values are shown for each plot.

The values of each age group's mPSD in each frequency band and each feeding period are shown in the bar plot in figure 1-9. The statistical analysis of these sample means included a single-factor ANOVA test followed by post-hoc pairwise t-tests and Tukey's Test. The error bars represent standard error of mean, which was calculated by taking the standard deviation across a GA group's curve and dividing it by the number of subjects in the group multiplied by the number of frequencies in a specific band. The full-term group shows significantly higher mPSD values than the premature babies in the during-feeding period for all three frequency bands. Moreover, the age groups show a linear increase in mPSD during-feeding across all bands, with full-term babies having a higher mPSD than mid-term babies, who had a higher mPSD than

early-term babies. The full-term group's mPSD is also significantly higher than that of the premature babies in the post-feeding period in all three frequency bands. However, mid-term subjects showed a higher mPSD than full-term subjects in the pre-feeding period for all three frequency bands.

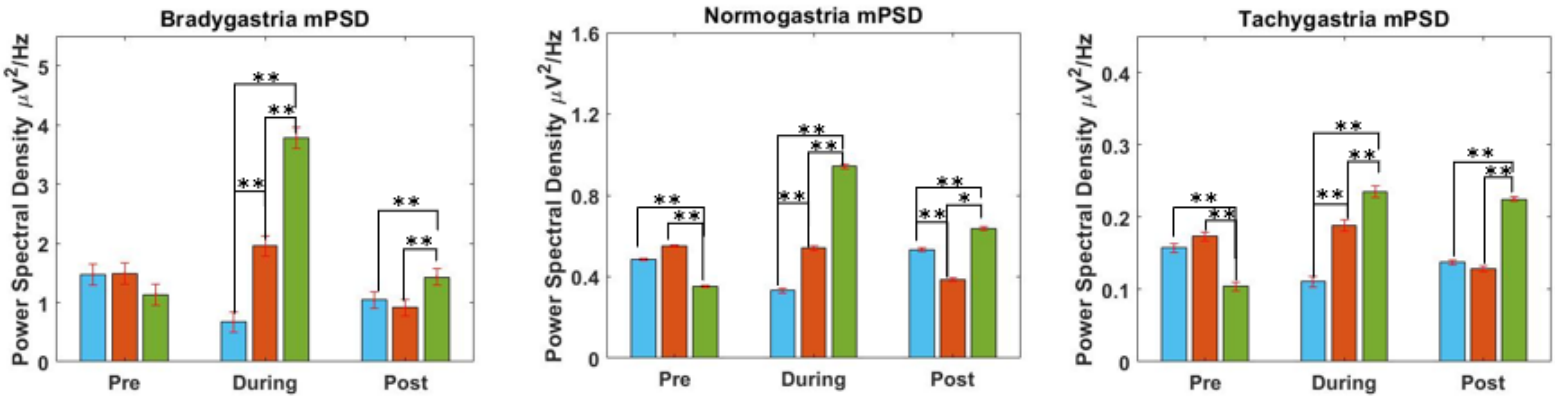

Figure 1-9: Bar graphs showing the difference in mPSD between age groups in bradygastria, normogastria, and tachygastria during the three feeding periods (pre-feeding, during-feeding, and post-feeding). The blue bars are the early-term group, the orange bar is the mid-term group, and the green bar is the full-term group. The error bars represent standard error of mean. The Bonferroni-adjusted p-value is 0.0167, and a single asterisk represents a p-value less than 0.0167. A double asterisk represents a p-value less than 0.00167.

1.3.4 Average Power Ratio Curves for Gestational Age Groups

The results of the averaged power ratio curves for both during-feeding and post-feeding are shown below in figure 1-10. The term-babies display a much higher power ratio curve in the during-feeding period than that of the premature infants. Additionally, there is significant difference between the curves of the early and mid-term groups in the normogastria band during the post-feeding period. These differences suggest that power ratio can be studied as a potential

marker that differentiates between premature and full-term neonates. This concept is further explored in the next section.

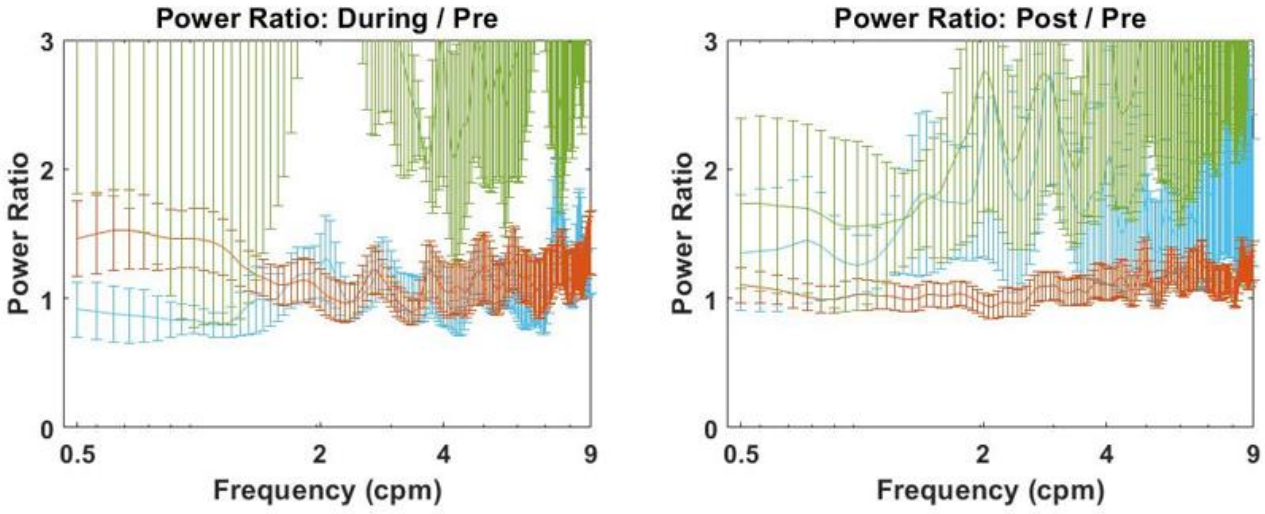

Figure 1-10: The average power ratio curves for the GA groups, with a logarithmic x-axis and a linear y-axis. The green curve denotes full-term babies, the red curve denotes mid-term babies, and the blue curve denotes early-term babies. The error bars represent standard error of mean.

1.3.5 Mean Power Ratio for Gestational Age Groups

The values of the curves in figure 1-10 were averaged within each band to calculate mean power ratio (mPR) for each age group. The group statistical analysis included single-factor ANOVA tests and post-hoc pairwise t-tests, as well as Tukey's Test. A bar graph of these mPR results is shown below in figure 1-11. A power ratio greater than 1 is considered to be a marker of good gastric motility (5).

1.3.5.1 Comparisons Between Neonate Groups

In all frequency bands and feeding-periods, full-term babies have a significantly higher mPR than premature babies. There are also significant differences between early and mid-term babies

in the post-feeding period, with early-term babies showing much higher mPR values than mid-term babies across all frequency bands.

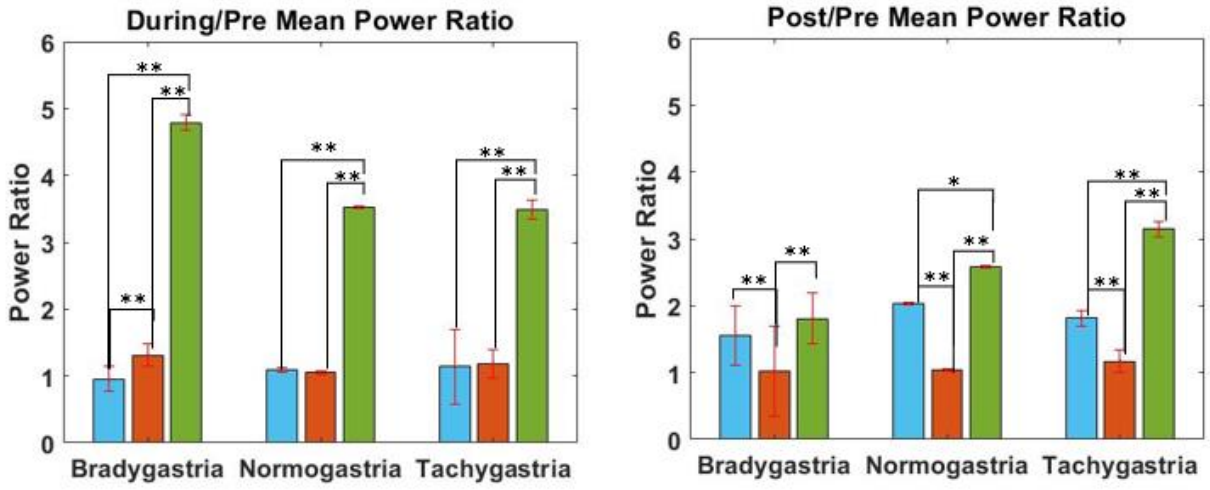

Figure 1-11: Bar graphs showing the group-level mean power ratio values. The power ratio of the during-feeding period is shown on the left, and the power ratio of the post-feeding period is shown on the right. The blue bars are the early-term group, the orange bar is the mid-term group, and the green bar is the full-term group. The error bars represent standard error of mean. The Bonferroni-adjusted p-value is 0.0167, and a single asterisk represents a p-value less than 0.0167. A double asterisk represents a p-value less than 0.00167.

1.3.5.2 Comparison with Adult Dataset

To further validate these results, an open-source EGG dataset with 20 healthy adults was downloaded from Zenodo and processed using the same methods described in section 1.2.3 (8, 9). This online dataset only included a pre-feeding and post-feeding period, so only its post-feeding power ratio has been considered and compared to the data in this study. The plot of the power ratio curves with all groups and this additional adult dataset is shown in figure 1-12. The

power ratio curve of the adults markedly jumps in the tachygastria band, and adults have higher power ratios as gastrointestinal frequencies increase.

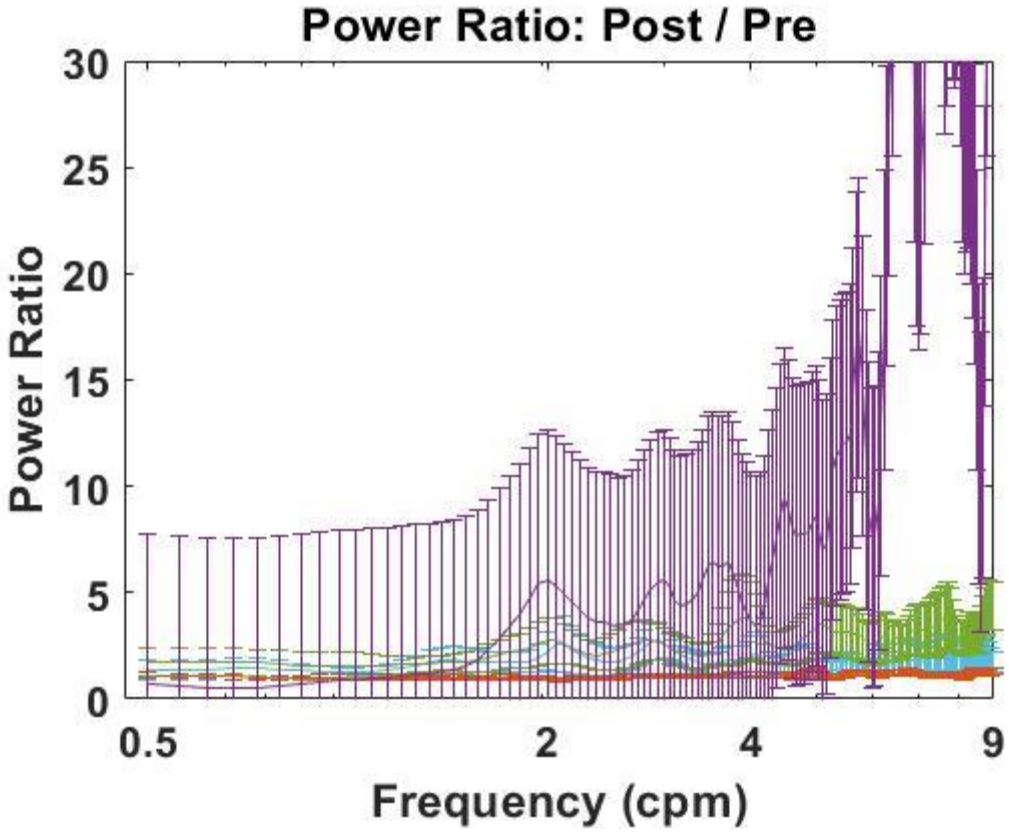

Figure 1-12: Power ratio curves for all three neonate age groups and the Zenodo dataset of 20 healthy adults, which is represented by the purple curve. The green curve represents full-term babies, the red curve represents mid-term babies, and the blue curve represents early-term babies. The x-axis has a logarithmic scale, while the y-axis has a linear scale.

The values of each curve in figure 1-12 were averaged in each band to calculate mPR values. After this, a single factor ANOVA test followed by post-hoc pairwise t-tests and Tukey tests were deployed for statistical analysis. The results are shown below in figure 1-13. In bradygastria, the adult group shows significant difference with regards only to the mid-term neonates. However, in both normogastria and tachygastria, the adult group has significantly higher mPR values than

every group of neonates. Section 1.3.5.1 noted that full-term babies have higher mPR values than premature babies; the adults' mPR values being even higher than those of the full-term babies suggests that EGG does indeed track developments in gastric motility as age increases from preterm to term babies and then to adults.

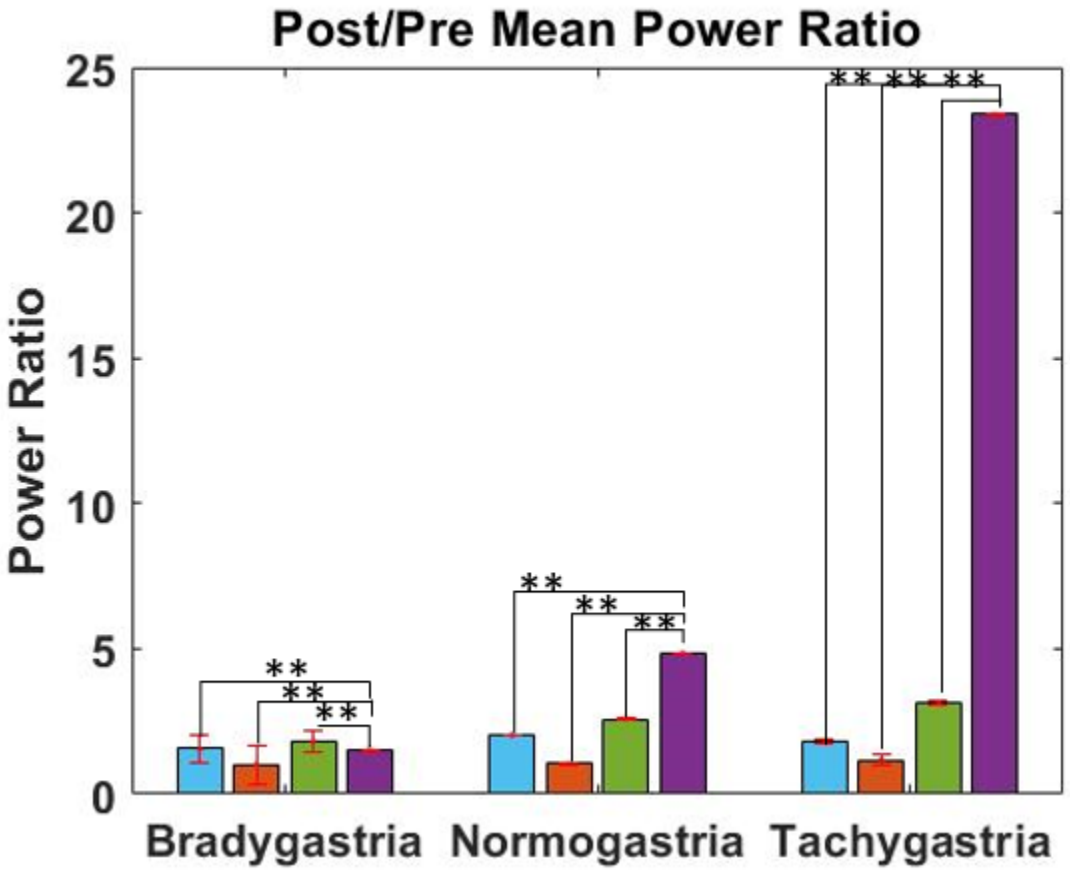

Figure 1-13: Bar plots showing the group averages for mPR, including the adult Zenodo dataset. Since comparisons between neonates have already been covered in the previous section, this figure only displays significant differences with regard to the adult dataset. The Bonferroni-adjusted critical p-value is 0.0125; a single asterisk represents a p-value less than 0.0125, while a double asterisk represents a p-value less than 0.00125.

1.3.6 Changes in Mean Power Ratio over Post-Menstrual Age

To further understand how the mean power ratio parameter evolves over age, the average mPR for each post-menstrual week of the overall cohort (n=77) was calculated and plotted below in figure 1-14. Not every patient had a recording in each week, so the number of babies included in each week's average varies. These numbers are shown at each datapoint. A red line has also been drawn at the y-intercept of 1 as a power ratio of 1 or higher has historically been considered as a marker of healthy gut motility.

Overall, it appears that mPR generally increases with post-menstrual age. In particular, patients with a very premature PMA (< 28 weeks) consistently show an mPR lower than 1. Then, at the 28 week mark and onward, mPR consistently remains above 1. This phenomenon is consistent with patterns of gut development in infants, wherein gut motility increases with age. These results show that EGG can track longitudinal changes in the gut with age, which has yet to be proven before in EGG data analysis.

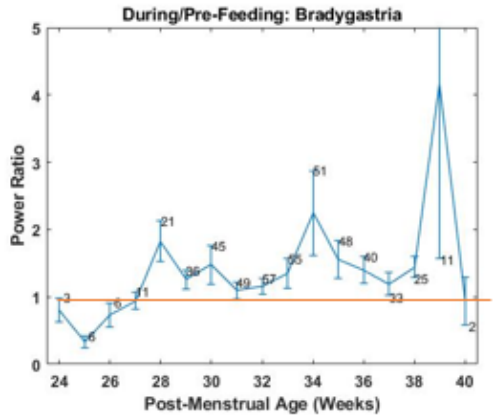

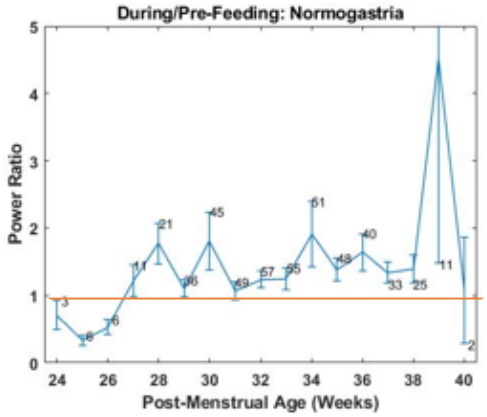

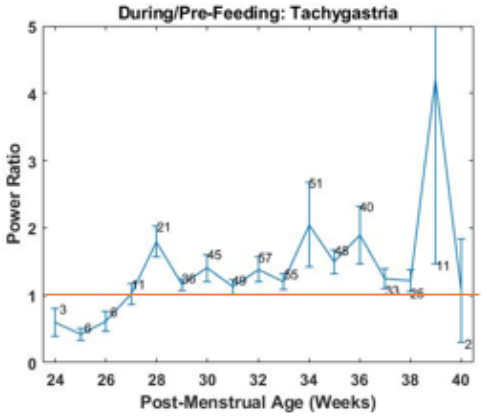

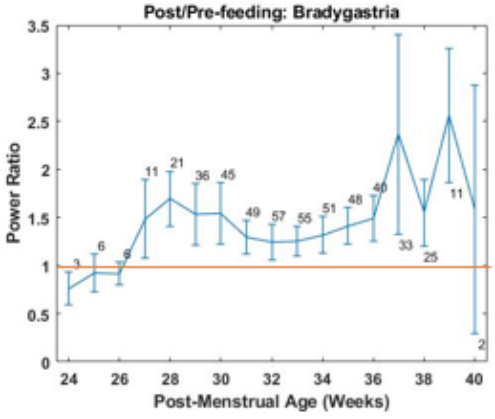

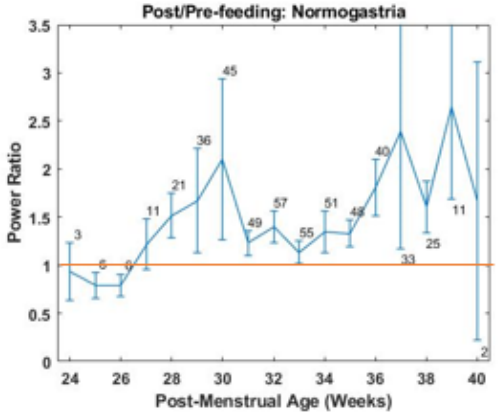

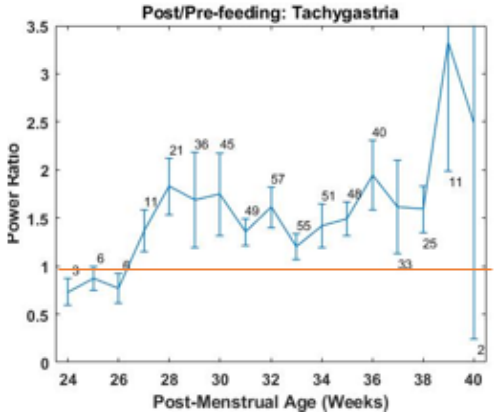

Figure 1-14: Plots for mean power ratio over post-menstrual age. The first row corresponds to the During-Feeding/Pre-Feeding power ratio, while the second row corresponds to the Post-Feeding/Pre-Feeding. The three columns for the plots also indicate the three gastric frequency bands.

1.3.7 Mean Power Ratio for Clinical Outcome of Feeding Intolerance

The dataset used in this study also included the clinical outcome of each baby. In particular, each baby was marked as having no feeding intolerance (n=57), developmental feeding intolerance (n=6), or pathological feeding intolerance (n=3). I stratified the babies into these 3 groups and calculated their power ratio curves (shown in figure 1-15) and their mPR bar plots (shown in figure 1-16).

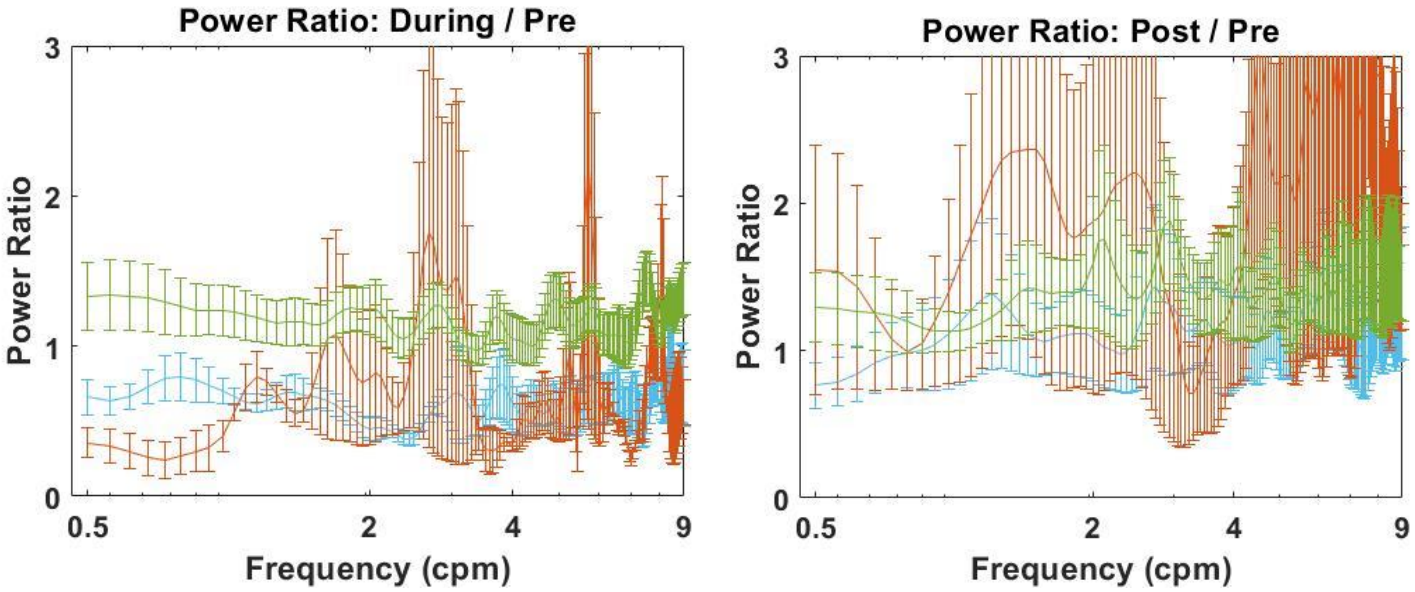

Figure 1-15: The power ratio curves for During-Feeding/Pre-Feeding (left) and Post-Feeding/Pre-Feeding (right).

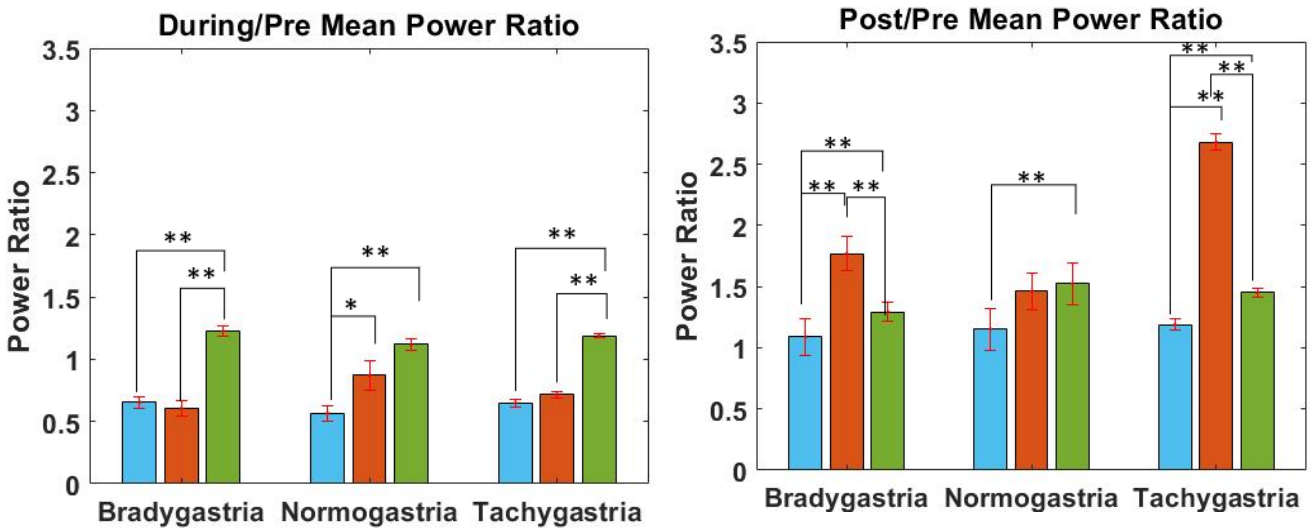

Figure 1-16: Bar plot for mPR of different feeding intolerance groups. The blue bars represent developmental feeding intolerance, the red bars represent pathological feeding intolerance, and the green bars represent no feeding intolerance.

These results show that the During-Feeding/Pre-Feeding power ratio can potentially distinguish between babies with feeding intolerance and babies without feeding intolerance, as the no feeding intolerance group consistently has a higher mPR. Additionally, the pathological feeding group has a higher mPR than both the developmental and no feeding intolerance groups in bradygastria and tachygastria for the Post-Feeding/Pre-Feeding power ratio. This suggests that babies with pathological feeding intolerance show a higher amount of gastric dysrhythmia after eating. Consequently, the power ratio parameter appears to be a useful tool in characterizing not only gut development with age, but feeding intolerance as well.

1.4 Discussion

As mentioned in the Introduction, quantification and application of EGG are understudied for clinical applications because of the lack of convincing results and peer-reviewed papers. One possible reason for such a situation is the large variability and inconsistency of the EGG data obtained; this problem could result from multiple factors, including different placement locations

of the electrodes, multiple signal sources that drive gastric myoelectrical activity, individual differences in patient health, and lack of transparent algorithms used to quantify EGG signals. All stated situations hold true for EGG applications in preterm newborns.

To overcome several of the aforementioned weaknesses, I chose a frequently used frequency-domain analysis method to determine the power spectral density (PSD) of the EGG data and examine whether the PSD spectra and frequency-band-averaged PSD (mPSD) values of early term, mid-term, and full-term newborns exhibited significant differences. One of the results in this part of my study demonstrated that PSD spectra and mPSD values were gestationally dependent, with the highest mPSD values in full-term babies across all three frequency bands (i.e., bradygastria, normogastria, and tachygastria).

In particular, I focused on a normalization method by quantifying the ratios between PSDs during vs. before feeding and between PSDs post vs. pre-feeding. This ratio method is particularly helpful because it is a self-calibration approach in which the pre-feeding EGG signal of each baby serves as his or her baseline for the ratio calculation. Thus, it can remove multiple systematic biases due to different electrode placement setups, personal health differences, and potential variations in the measurement conditions. My results demonstrated that this ratio method is simple and effective for identifying distinct features among babies with different gestational ages. The ratio method is expected to be effective in characterizing newborns longitudinally at different postmenstrual ages (PMA). The analysis of this set of data is ongoing, and the results are expected to provide PMA-dependent EGG power ratio changes that may serve as markers of gastric health and development of newborns.

CHAPTER 2

Prefrontal Hemodynamic and Metabolic Coherence in Healthy Older Adults

2.1 Introduction

The prefrontal cortex of the brain serves high-order cognitive functions, including emotional regulation and working memory (15). Reduced blood oxygenation in this cortex has been historically observed in adults with Alzheimer's, a disease which affects over six million Americans (16, 17). In the face of this staggering number, there has been an increasing focus on studies about the prefrontal cortex's role in the development of Alzheimer's. Consequently, the creation of new methods for calculating different prefrontal biomarkers is an important part of understanding Alzheimer's Disease (AD), especially when considering the resting-state of individuals with AD.

The non-invasive optical tool of broadband Near-Infrared Spectroscopy (bbNIRS) has long been established to measure changes in oxygenated hemoglobin (HbO) (13). However, for the past several years, our lab has also established an algorithm to calculate changes in cytochrome C oxidase (CCO), an enzyme that helps regulate ATP synthesis (18). Consequently, it is now possible to analyze how HbO and CCO interact at the cellular level, especially in the case of older adults who are at higher risk of developing AD. To look at this interaction, this study is focused on calculating coherent coefficients between HbO and CCO signals in healthy older adults. These coefficients are further analyzed in different frequency bands to determine their physiological implications in the prefrontal cortex.

Infra-slow oscillations (ISO) are vascular rhythms in the brain associated with contraction cycles in different layers of cortical vessels. These rhythms are classified into three

frequency bands: endogenic (0.005 - 0.02 Hz), neurogenic (0.02 – 0.04 Hz), and myogenic (0.04 – 0.2 Hz) (19). The endogenic band supplies information about the dilation-contraction cycles of the endothelial layer, which are responsible for the release of vasoactive factors such as nitric oxide, free radicals, and endothelin (20). Furthermore, oscillations in the neurogenic band are associated with neurotransmitter and vasoactive ion release from neurons, which controls the dilation-contraction cycles of blood vessels (20). Lastly, the myogenic band contains the activity of relaxation-contraction cycles of the smooth muscle that surrounds blood vessels (20). Changes in oxygenated hemoglobin and mitochondrial activity in these bands can potentially quantify differences in brain processes between healthy older adults and older adults with Alzheimer's Disease.

Furthermore, the amplitude of the HbO and CCO signals in the ISO bands can provide additional information about the brain's ability to address hemodynamic and metabolic demands from different layers of cerebral vasculatures. Consequently, spectral amplitudes of these signals were also calculated and averaged in this study. The methodology used in the current study is patterned after that of Shahdadian et. al. in 2022, which took bbNIRS readings from young adults aged 18-24. Consequently, the current study seeks to compare the aforementioned parameters of a preliminary sample (n=6) of older adults with the young adults used in the study from Shahdadian et. al.

2.2 Methodology

2.2.1 Experimental Setup

The study was approved by the IRB and took place from June to September 2022 at UTA's Science and Engineering Innovation Research building. Recruitment for the study was handled

by our collaborators in the School of Social Work in Dr. Kathy Lee's lab. The recruitment targeted adults over the age of sixty with no diagnosis or symptoms of dementia and/or AD to serve as a control group for future participants with AD. A total of six participants were recruited in the study. All participants read and signed informed consent forms prior to their measurements. For additional information, all participants were given instructional videos and a pamphlet about the experimental procedure, as well as the purpose of the study. All participants abstained from caffeine, alcohol, and exercise during the 12 hours leading up to their scheduled measurement. The study included five females and one male, with an average age of 64.7 ± 3.4 years.

2.2.2 Experimental Protocol

Each subject had one measurement, which included a 14 minutes and 10 seconds recording period of bbNIRS and EEG data. Since the primary focus of the current study is about hemodynamic-metabolic coherence, the EEG data has been excluded. The length of the measurement included seven minutes wherein the subject's eyes were open, seven minutes with the subject's eyes closed, and ten seconds between the two periods to allow for transition into the eyes-closed stage. This ten second interval was excluded from analysis. Furthermore, during the eyes-open stage, subjects were instructed to keep their eyes focused on a rectangular piece of black tape on the wall opposing them to reduce eye motion artifact. The tape was placed at eye-level during the set-up period in order to prevent neck strain. Images of the experimental setup are shown below.

Figure 2-1: The setup of the EEG in conjunction with bbNIRS.

Figure 2-2: A close-up image of the Quick-20 EEG and bbNIRS headband.

2.2.3 Broadband Near-Infrared Spectroscopy

The bbNIRS system consisted of two-channels, to acquire data from each cortical hemisphere. Both of the light sources were Tungsten halogen lamps that emitted broadband white light (Model 3900e, Illumination Technologies, NY, USA). The two optical detectors were CCD-array spectrometers (QEPRO, Ocean Optics Inc., Orlando, FL, USA). Each spectrometer's integration time was set at 1.5 seconds, resulting in a 0.67 sampling frequency. Optical fibers connected the lamps and detectors to a 3-D printed headband, shown in figure 2-2, which was then placed on the subject's forehead. The headband included divots to allow room for the EEG's prefrontal electrodes.

2.2.4 Electroencephalogram

The EEG used in this study was a 19-channel, dry headset controlled by Bluetooth (Quick-20, CGX Systems, San Diego, CA, USA). The 20th channel, A2, was only used for the contralateral referencing of the scalp electrodes, and so it was removed from the dataset. The EEG data was excluded from the results and analysis of the current study.

2.2.5 Spectral Amplitude Calculation Using the Multi-Taper Method

The correlation between the amplitudes and phases of different channels on the scalp can be used to calculate connectivity within the brain. In the case of the dual-channel bbNIRS, the collected HbO and CCO time series can be decomposed into spectral amplitude and phase. The spectral amplitude of each signal can then be averaged to conduct group-level analyses of hemodynamic and metabolic spectral amplitude, respectively. The amplitude and phase decomposition was done using the following method: first, a multi-taper method followed by Fast Fourier Transform (mtm-fft) was applied to the time series data. This is a prominent spectral analysis method that reduces the variance of spectral estimates of a signal by applying tapers (21). In this case, the

tapers were Slepian sequences, which is a window with maximal energy concentrated in the main lobe to increase resolution (22). After applying the mtm-fft method, the power spectra were averaged to a single value in each infra-slow oscillation band, which has been termed as each group's spectral amplitude. This process was done for four time series signals to calculate the spectral amplitude of (1) HbO on the left-side of the forehead, (2) HbO on the right-side of the forehead, (3) CCO on the left-side of the forehead, and (4) CCO on the right-side of the forehead.

2.2.6 Coherence Calculation

The cross-correlation between two signals in the time domain is the equivalent of their coherence in the frequency domain. This coherence is quantified between 0 and 1 by the following equation from Bastos and Schoffelen (23):

$$coh_{xy}(\omega) = \frac{\left|S_{xy}(\omega)\right|}{\sqrt{S_{xx}(\omega)S_{yy}(\omega)}}$$

In this equation, x and y are the two signals, Sxx and Syy are their power estimates, and Sxy is the cross-spectral density term of the two input signals. Each of these terms were calculated using the aforementioned mtm-fft method. Then, the imaginary part of coherence was calculated using the FieldTrip toolbox (21). This creates four parameters: (1) the bilateral coherence of HbO, (2) the bilateral coherence of CCO, (3) the unilateral coupling of HbO and CCO on the left-side of the forehead, and (4) the unilateral coupling of HbO and CCO on the right-side of the forehead.

2.3 Results

The following two tables display the average spectral amplitude (SA) values and their standard deviations for HbO and CCO in each of the ISO frequency bands. After averaging was conducted, a two-tailed, paired t-test was calculated between the left and right values for HbO and CCO, respectively. The resulting p-value is shown in the rightmost column in these tables. Overall, there was no statistically significant difference between the average spectral amplitudes of the left and right sides of the prefrontal cortex.

Frequency Band	$SA_{HbO,left}$	$SA_{HbO,right}$	Left vs. Right t-test (p-value)
Endogenic	0.18 ± 0.14	0.11 ± 0.03	0.294
Neurogenic	0.096 ± 0.11	0.063 ± 0.05	0.332
Myogenic	0.024 ± 0.01	0.023 ± 0.01	0.721

Table 2-1: SA values for oxygenated hemoglobin averaged across all six subjects.

Frequency Band	$SA_{CCO,left}$	$SA_{CCO,right}$	Left vs. Right t-test (p-value)
Endogenic	0.016 ± 0.011	0.015 ± 0.007	0.749
Neurogenic	0.009 ± 0.011	0.009 ± 0.006	0.836
Myogenic	0.005 ± 0.001	0.005 ± 0.001	0.595

Table 2-2: SA values for cytochrome C oxidase averaged across all six subjects.

The subsequent two tables show the averaged bilateral coherence values for HbO and CCO (table 2-3) and the averaged unilateral coherence values for HbO and CCO on the left and right sides of the prefrontal cortex (table 2-4), as well as the standard deviation of these parameters. After averaging, a two-tailed, paired t-test was applied to each pair of frequency bands (i.e. endogenic vs. neurogenic, neurogenic vs. myogenic, and endogenic vs. myogenic). Two statistically significant differences (p-values less than 0.05) were found for: (1) $bCON_{HbO}$ between the neurogenic and myogenic bands, and (2) $uCOP_{HbO\text{-}CCO,left}$ between the endogenic and

myogenic bands. These statistically significant p-values are shown in the rightmost columns of these tables.

Frequency Band	$bCON_{HbO}$	$bCON_{CCO}$	$bCON_{HbO}$ t-test (p-value), N vs. M
Endogenic	0.69 ± 0.11	0.49 ± 0.16	0.045
Neurogenic	0.73 ± 0.05	0.42 ± 0.20	
Myogenic	0.58 ± 0.12	0.36 ± 0.06	

Table 2-3: Coherence values for bilateral coupling of oxygenated hemoglobin and cytochrome C oxidase, averaged across all six subjects.

Frequency Band	$uCOP_{HbO\text{-}CCO,left}$	$uCOP_{HbO\text{-}CCO,right}$	$uCOP_{HbO\text{-}CCO,left}$ t-test (p-value), E vs. M
Endogenic	0.60 ± 0.18	0.49 ± 0.16	0.034
Neurogenic	0.44 ± 0.24	0.46 ± 0.19	
Myogenic	0.42 ± 0.07	0.44 ± 0.08	

Table 2-4: Coherence values for unilateral coupling of oxygenated hemoglobin and cytochrome C oxidase, respectively, on the left and right sides of the forehead, averaged across all six

2.4 Discussion

Since this study uses the same methodology as that by Shahdadian et. al., it is imperative to compare our results for the range of the four amplitude and coherence parameters to those published for a younger group. In particular, our older adult population had lower values in $SA_{HbO,left}$, $SA_{HbO,right}$, and $SA_{CCO,left}$ in the myogenic band when compared to the younger adults. Additionally, they had higher values in $uCOP_{HbO\text{-}CCO,left}$ in the endogenic and myogenic bands, as well as in $uCOP_{HbO\text{-}CCO,right}$ in the myogenic band. A table summarizing these differences is shown below in table 2-5.

	$SA_{HbO,left}$	$SA_{HbO,right}$	$SA_{CCO,left}$	$SA_{CCO,right}$	$bCON_{HbO}$	$bCON_{CCO}$	$uCOP_{HbO-CCO,left}$	$uCOP_{HbO-CCO,right}$
Endogenic	-	-	-	-	-	-	Increase	-
Neurogenic	-	-	-	-	-	-	-	Increase
Myogenic	Decrease	Decrease	Decrease	-	-	-	Increase	-

Table 2-5: A comparison between older adults (the current study) and younger adults (Shahdadian et. al.) in the 8 parameters for prefrontal hemodynamic-metabolic coherence. A "-" represents no difference between the two groups (i.e. the values in the current study fall within the ranges determined by Shahdadian et. al.). "Increase" means that the older adults have a value higher than the younger adults, and "Decrease" indicates that they have a lower value than the younger adults.

The overall decrease in spectral amplitude in the myogenic band suggests that the intensity of smooth muscle contractions decrease with age. The structure of the vascular wall significantly changes with age, as smooth muscle cell hypertrophy and changes in collagen density stiffens the wall (24). Additionally, the B-adrenoceptor-mediated relaxation of smooth muscle and the contractile response to alpha-adrenoceptor agonists decreases with age (24). Consequently, as humans age, it is, in essence, harder for the smooth muscle to contract and relax. This resistance may be the cause of the lower SA values in the myogenic band across older subjects.

Furthermore, unilateral hemodynamic-metabolic coupling is associated with the supply and demand between local (i.e. left or right hemisphere) hemodynamics and metabolism (20). Lower levels of connectivity in the hippocampal-prefrontal cortex have been noted in disorders with cognitive deficits, such as major depression and AD (x). Consequently, low values of bilateral connectivity or coupling can potentially indicate markers of cognitive issues. In the

current study, however, the older adults had significantly higher levels of unilateral coupling than the younger adult population. This result is partly expected, as the older adults included in the current study have not been diagnosed with AD or shown any cognitive deficits. It is not peculiar that the population does not have an inherently lower rate of unilateral coupling. However, the sample size of the current study was six with one measurement each, and it is being compared with 26 younger subjects with five measurements each. Further measurements of healthy older adults could provide a more precise range for unilateral coupling values, which may bring it closer to the ranges described by Shahdadian et. al.

Therefore, the current study is limited in sample size. Future work should involve taking more measurements and, potentially, taking multiple measurements from each subject over the course of 5 weeks, as was done in the study by Shahdadian et. al. Furthermore, it would be very useful to collect resting-state data from older adults diagnosed with AD in order to paint a more robust picture of what SA and connectivity values look like in older populations. We generally expect patients with AD to show lower connectivity values, whether globally in bilateral connectivity or locally in unilateral coupling, due to the cognitive impairments that come with the disease. Additionally, we would also expect them to have similarly lower SA values in the myogenic band due to the aforementioned age-related changes in the structure of the vascular wall. Although the current study was confined to six subjects, the values described in this paper indicate a future direction for the trend of prefrontal hemodynamic-metabolic connectivity in the elderly.

CHAPTER 3

Wavelet Transform Coherence for Analysis of Hemodynamic-Metabolic Activity

3.1 Introduction

The prevalence of cardiovascular disease in different races is a phenomenon that has long been investigated. It is of particular interest to study how early signs of hypertension and cardiovascular disease manifest in disproportionately affected races. A standard test to assess such vascular activity, as well as tissue perfusion, is a Vascular Occlusion Test (VOT) (10). By restricting blood flow to a limb, often chosen to be the forearm, changes in blood oxygenation levels are recorded. In a healthy subject, blood oxygenation is expected to increase just after occlusion, decrease as the occlusion is sustained, and significantly increase once the occlusion is removed (11). Significant deviation from this pattern is considered abnormal, and it could potentially quantify a racial disparity in cardiovascular health.

Furthermore, Near-Infrared Spectroscopy, or NIRS, is most commonly used during VOTs due to its non-invasive nature and ability to measure oxygen saturation in hemoglobin. In particular, Broad-band NIRS (bbNIRS) features a wider and more inclusive range of near-infrared wavelengths, which allows it to quantify another biological feature: metabolism. In the past, bbNIRS has been used to measure changes in cytochrome C oxidase (CCO), a key enzyme in the mitochondrial electron transport chain and, by extension, ATP synthesis. Thus, by measuring changes in CCO, we are able to investigate metabolic changes in the body during a VOT. These changes could broaden the scope of cardiovascular research and highlight physiological features in populations with higher rates of cardiovascular disease and hypertension.

However, there are many analysis methods for the signals that bbNIRS can measure. This study seeks to investigate a newer method called Wavelet Transform Coherence (WTC), which reveals both temporal and spectral characteristics of the coherence between two signals. Though it was initially developed for usage in geological research, it is especially applicable to biomedical research. Other frequency domain-specific tools often applied in biomedical research, such as Fast Fourier Transform, are limited to spectral analysis alone. However, physiological signals, like oxygenated hemoglobin (HbO), are stochastic in nature. Therefore, WTC provides robust analysis by allowing its users to look at how these physiological signals change over time. In particular, WTC gives more insight into how VOTs can influence the relationship between blood oxygenation and metabolism. WTC-generated heat maps show the specific time and frequency ranges at which these signals are coherent, providing visual data as to how these biological functions work, as shown in figure 3-1. Additionally, there are three characteristic infraslow frequency bands that can be analyzed from HbO and CCO data: endogenic, neurogenic, and myogenic (12). The endogenic band is associated with the endothelial layer's release of nitric oxide, prostacyclin, and endothelin. The neurogenic band, however, is related to oscillations from the release of neurotransmitters and vasoactive ions for vessel dilation-contraction cycles. Lastly, the myogenic band infers information about relaxation-contraction cycles of vascular wall smooth muscle cells. Therefore, by looking at the coherence between HbO and CCO in these bands, we can observe the impact of hemodynamic-metabolic activity on the release of vasoactive factors in the endothelial layer, neurotransmitter release in the peripheral nervous system, and smooth muscle contraction.

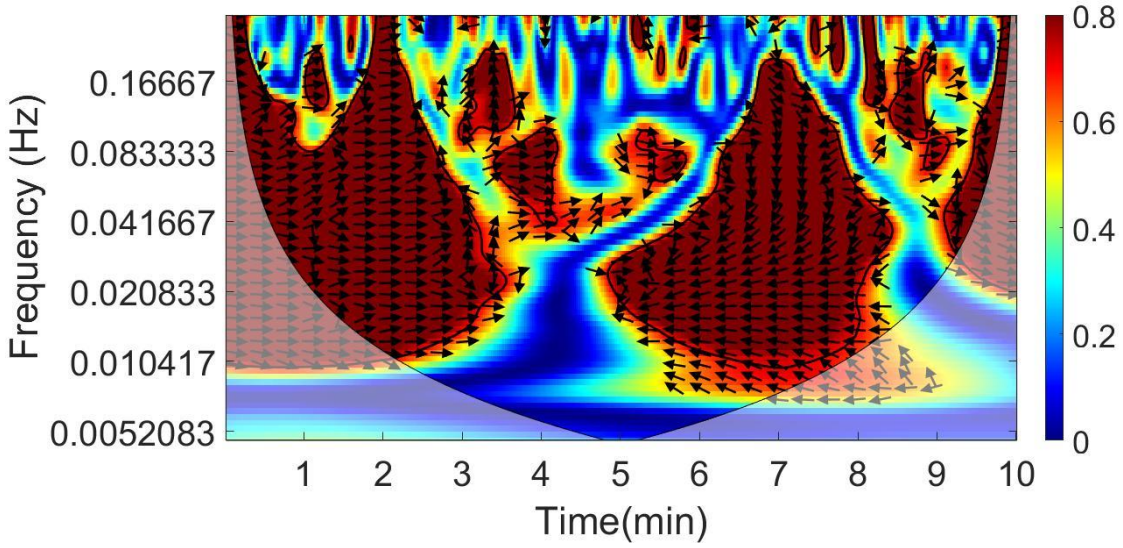

Figure 3-1: An example of a WTC heat map. The x-axis represents time and the y-axis represents frequency. The color bar for coherence is displayed on the right; with 0.8 representing significant coherence.

Consequently, the purpose of this study was to establish a baseline of WTC heat maps between HbO and CCO signals in healthy adults during a VOT. These maps can thus indicate what normal coherence between these signals looks like, and they can also be used as a reference point for comparison with populations at risk of developing cardiovascular disease. Furthermore, WTC has not yet been applied to HbO and CCO signals as determined from bbNIRS data, which makes this study novel. Therefore, this study seeks to investigate both the efficacy of WTC in analyzing hemodynamic-metabolic activity and potential baselines for this activity.

3.2 Methods

3.2.1 Experimental Design

A preliminary study using a VOT on seven healthy adult subjects was conducted from August to September in 2022. Five of the subjects had more than one measurement, with one reading being taken from each of their forearms. In particular, two subjects had three

measurements, and three subjects had two measurements. During the setup for the experiment, subjects laid down and relaxed their arm before an automatic arm cuff was placed on their forearm, just past their brachial artery. Then, an OceanOptics bbNIRS spectrometer was placed further up their wrist, as shown below in figure 3-2.

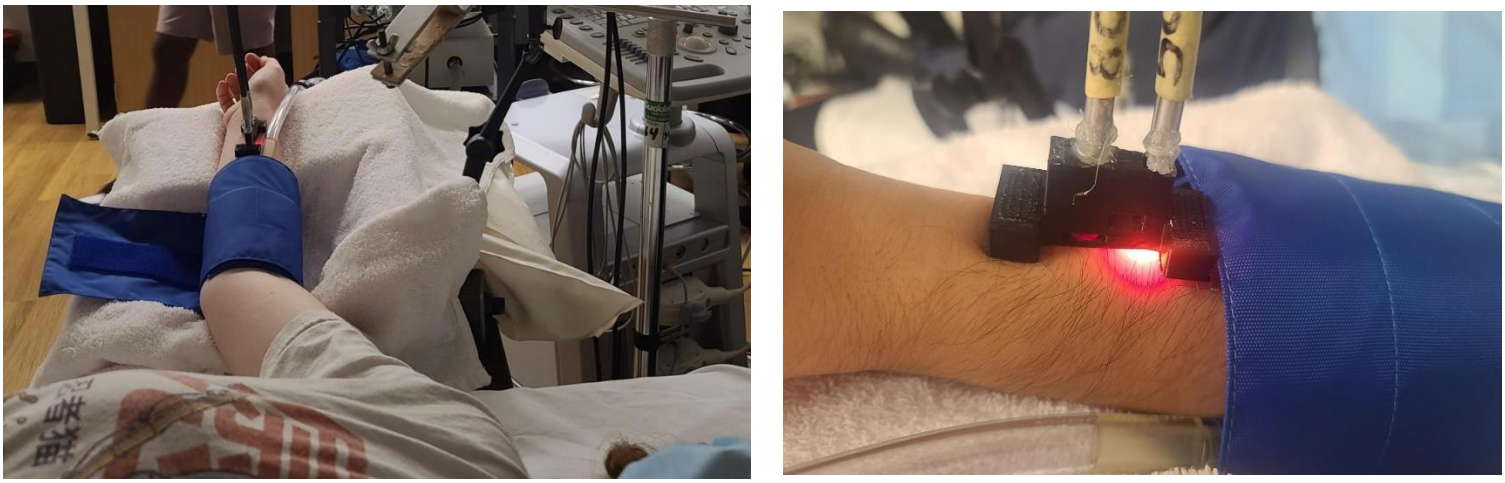

Figure 3-2: An image of the arm cuff and bbNIRS placement.

The experimental protocol was as follows: first, two minutes were allowed for baseline, in which the arm cuff was off and the subject remained at rest. Then, the arm cuff restricted with a pressure of 220 T to induce ischemia in the forearm. This occlusion was sustained for five minutes, except in the cases of subjects 6 and 7, whose forearms were occluded for three minutes. Lastly, the arm cuff was loosened and three minutes of recovery were recorded. Subjects 6 and 7 had a recovery time of five minutes. Each measurement lasted for ten minutes.

3.2.2 bbNIRS Data Processing

Data from the spectrometer was processed in MATLAB to calculate changes in HbO and CCO directly following the methodology established by Wang et. al for changes in three chromophores in the forearm (13). The methodology involves an extinction coefficient matrix of

tissues in the forearm under the band of wavelengths outputted by the bbNIRS device, as well as multiple linear regression analysis to select optimal fits for HbO, CCO, and HHb (deoxygenated hemoglobin). The HHb values are outside of the scope of this study, which is concerned with the coherence between HbO and CCO, and so they have been excluded for future analysis.

3.2.3 Wavelet Transform Coherence

The WTC methodology is based on Continuous Wavelet Transform (CWT), a method for calculating an overcomplete representation of a time-domain signal. A Morlet wavelet, or a Gaussian-windowed sinusoid, was deployed in our CWT calculations due to its usage in Grinsted's code for WTC (14). The Gaussian nature of the Morlet wavelet allows it to weigh each point in time during the convolution process of the Fourier transform; this key feature retains both time and frequency information during convolution. Consequently, CWT was applied to both the HbO and CCO signals. Then, the cross-correlation between these two signals was calculated, creating a coherence value at different frequencies at each point in time. These coherence values were mapped to a color bar ranging from blue to red, with red representing the maximum coherency in the plot. As an example, figure 3-1 shows this heat map.

Additionally, black contour lines are drawn around areas of significant coherence within the heat map. Black arrows appear within these areas of significance to indicate the phase difference between the two input signals. An arrow pointing right represents a 0-degree difference, such that the signals are completely in-phase. Similarly, an arrow pointing up represents a 90-degree difference, a leftwards direction represents a 180-degree difference (or anti-phase behavior), and a downward arrow represents a 270-degree difference.

Lastly, the shadowed area at the edge of the heat maps represents the Cone of Interference (COI). Due to the tapered nature of the Morlet wavelet, padded zeros are added onto each signal before convolution to ensure that the first time-series point is included during Fourier Transform. Consequently, the data at the edges of the continuous wavelet-transformed signals are not true results of convolution; therefore, they are depicted as points within the COI and are not considered in the analysis of WTC heat maps.

3.3 Results

The following figures display the heat maps between HbO and CCO for all seven subjects. In particular, there appears to be significant coherence at the end of the baseline period and into the first minute of forearm occlusion in the entirety of the neurogenic band, as well as in the first half of the myogenic band. In all but one subject (subject 3), this coherence is almost entirely in-phase. There is a similar pattern of coherence during occlusion (from 2 to 7 minutes) in the neurogenic band and part of the myogenic band, and it tends towards the 270 degree phase difference and complete anti-phase behavior in all but three subjects. These results suggest that ischemic conditions induce anti-phase behavior during smooth-muscle contractions and the release of neurotransmitters for vessel dilation-contraction cycles.

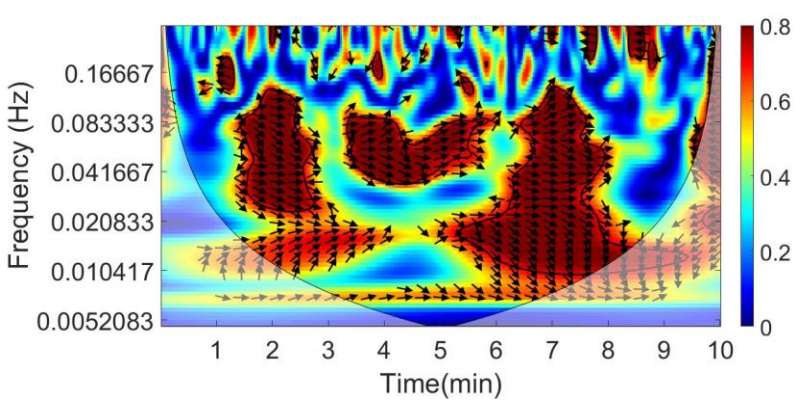

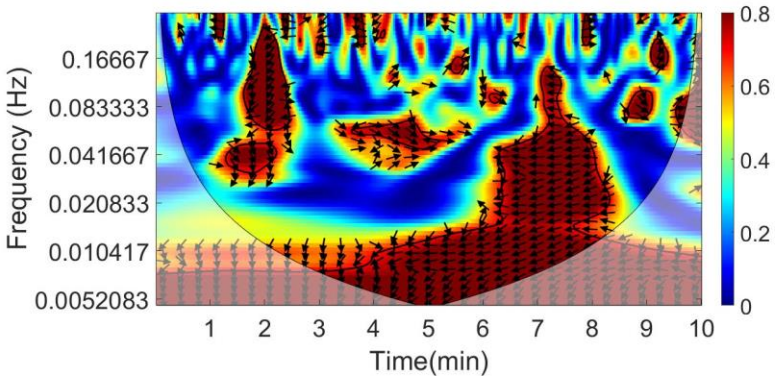

Figure 3-3: Subject 1's heat maps, including the left forearm (left) and right forearm (right).

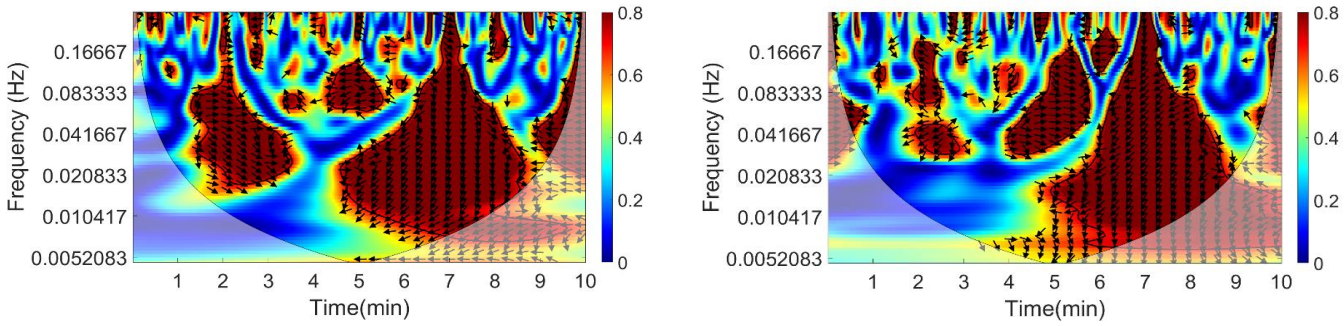

Figure 3-4: Subject 2's heat maps, including the left forearm (left) and right forearm (right).

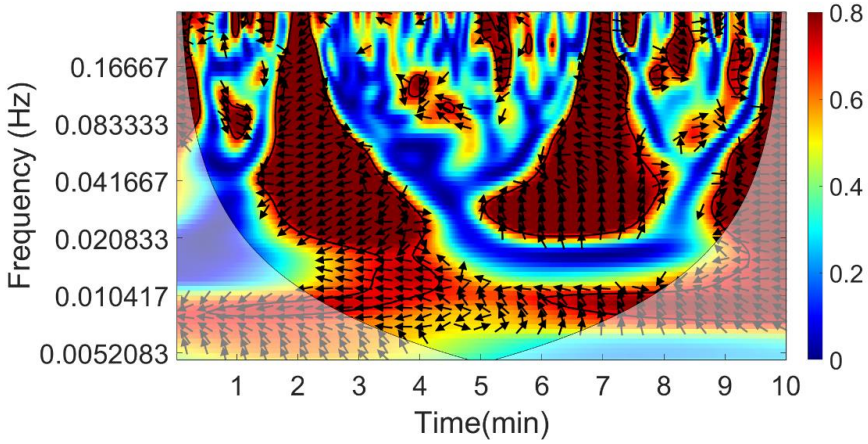

Figure 3-5: Subject 3's heat map for the left arm.

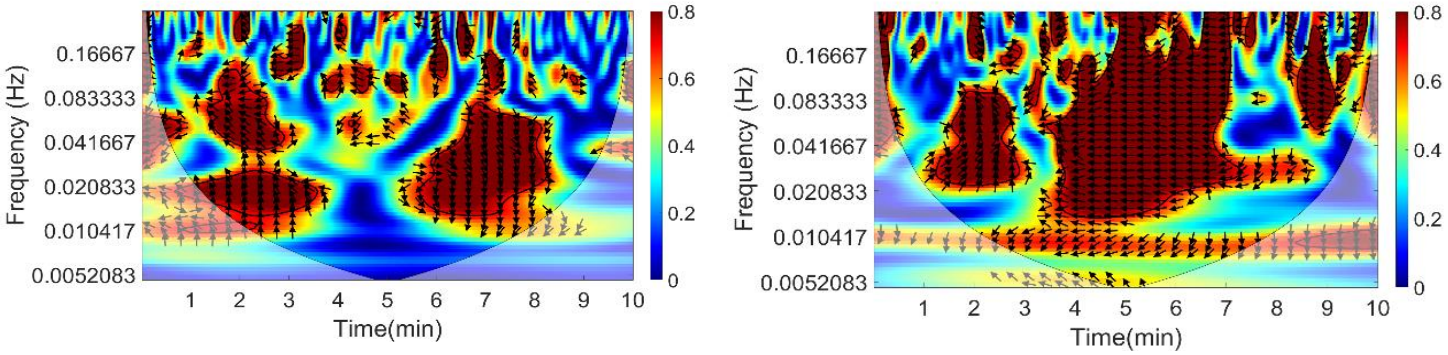

Figure 3-6: Subject 4's heat maps, including the left forearm (left) and right forearm (right).

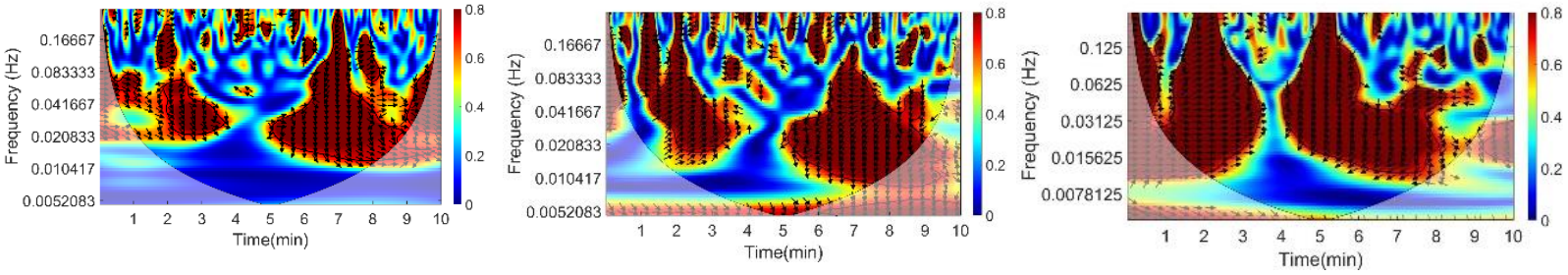

Figure 3-7: Subject 5's heat maps, including the left forearm (left), right forearm (middle), and a repeated measurement of the right forearm (right).

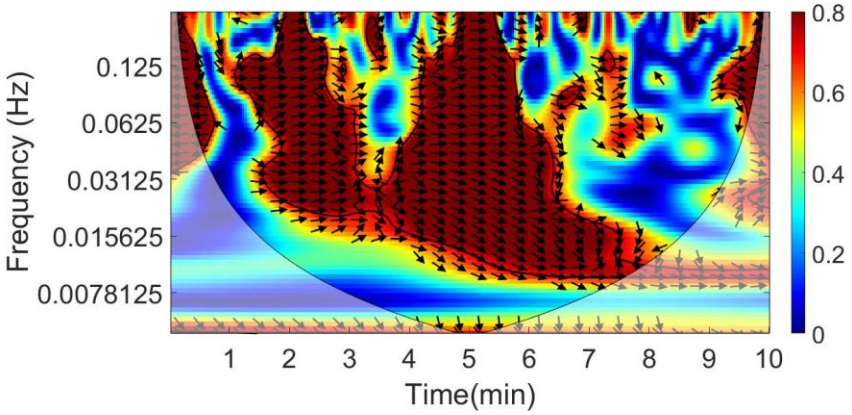

Figure 3-8: Subject 6's heat map for the left arm.

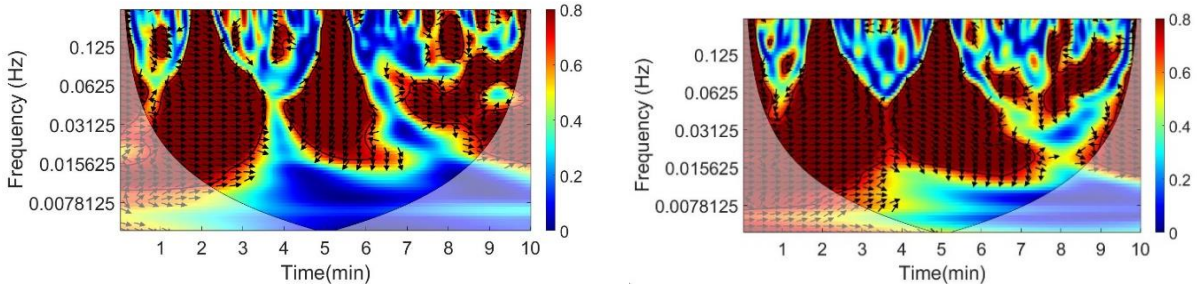

Figure 3-9: Subject 7's heat maps, including the left forearm (left) and right forearm (right).

Additionally, the time series of HbO, HHb (deoxygenated hemoglobin), and CCO for each subject is shown below. The expected decrease in HbO and increase in HHb is observed once occlusion begins at the 2 minute mark. However, the changes in the CCO signal were less consistent. In 5 subjects, CCO generally increased at the start of occlusion, then plateaued at that value until the arm cuff was released. In the other two subjects, subjects 3 and 4, CCO steadily increased (in the case of subject 3) or decreased (in the case of subject 4).

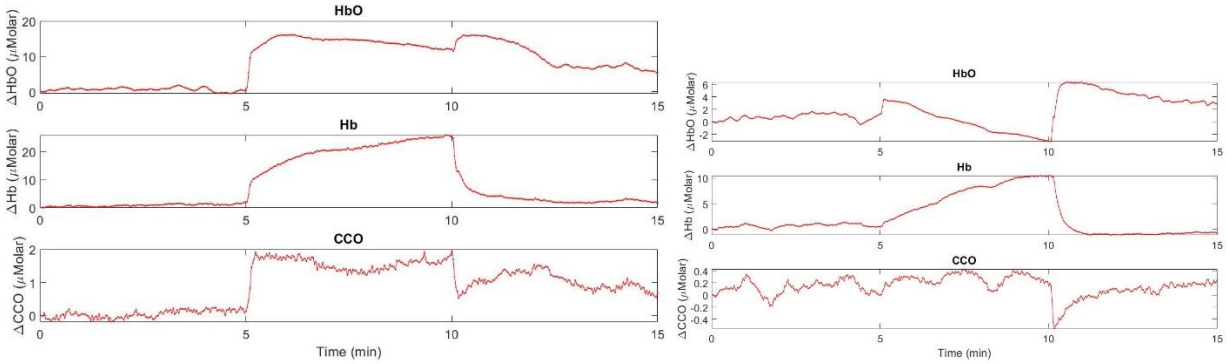

Figure 3-10: Subject 1's HbO, HHb, and CCO time series for the left forearm (left) and right forearm (right).

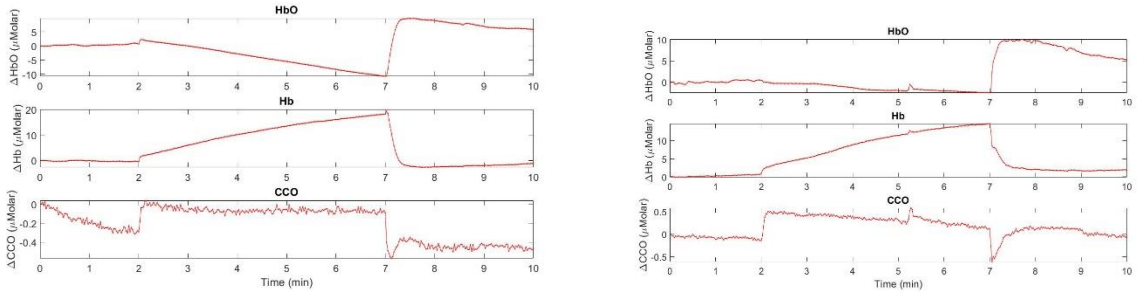

Figure 3-11: Subject 2's HbO, HHb, and CCO time series for the left forearm (left) and right forearm (right).

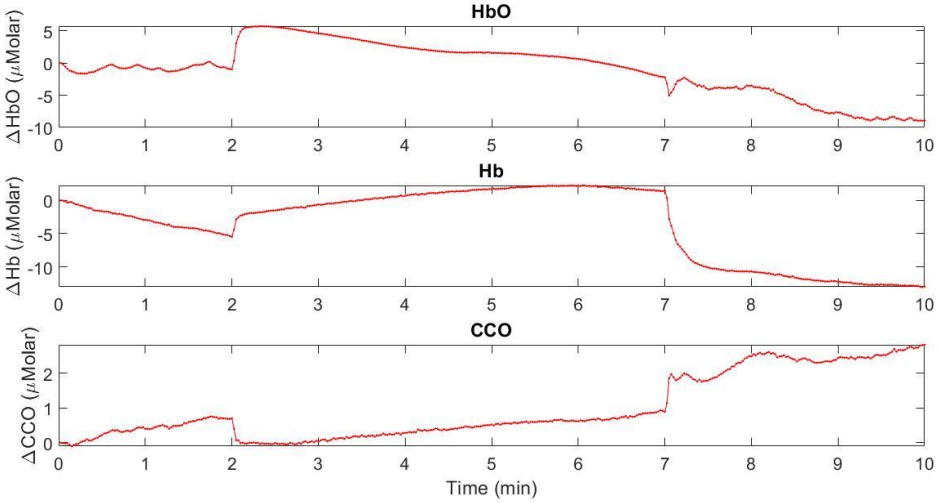

Figure 3-12: Subject 3's HbO, HHb, and CCO time series for the left forearm.

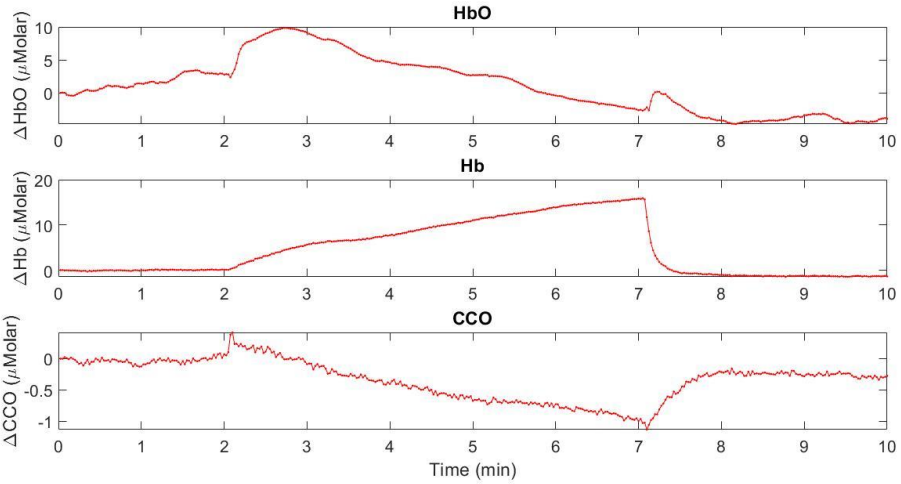

Figure 3-13: Subject 4's HbO, HHb, and CCO time series for the left forearm.

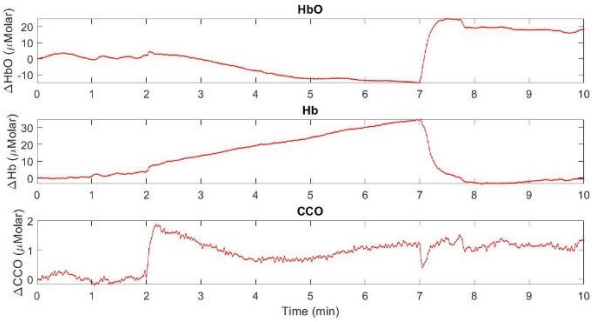

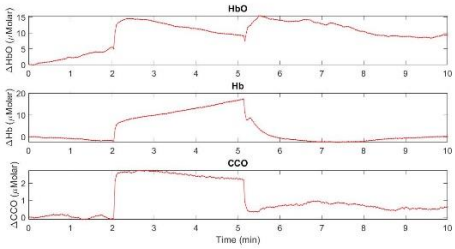

Figure 3-14: Subject 5's HbO, HHb, and CCO time series for the left forearm (left) and right forearm (right).

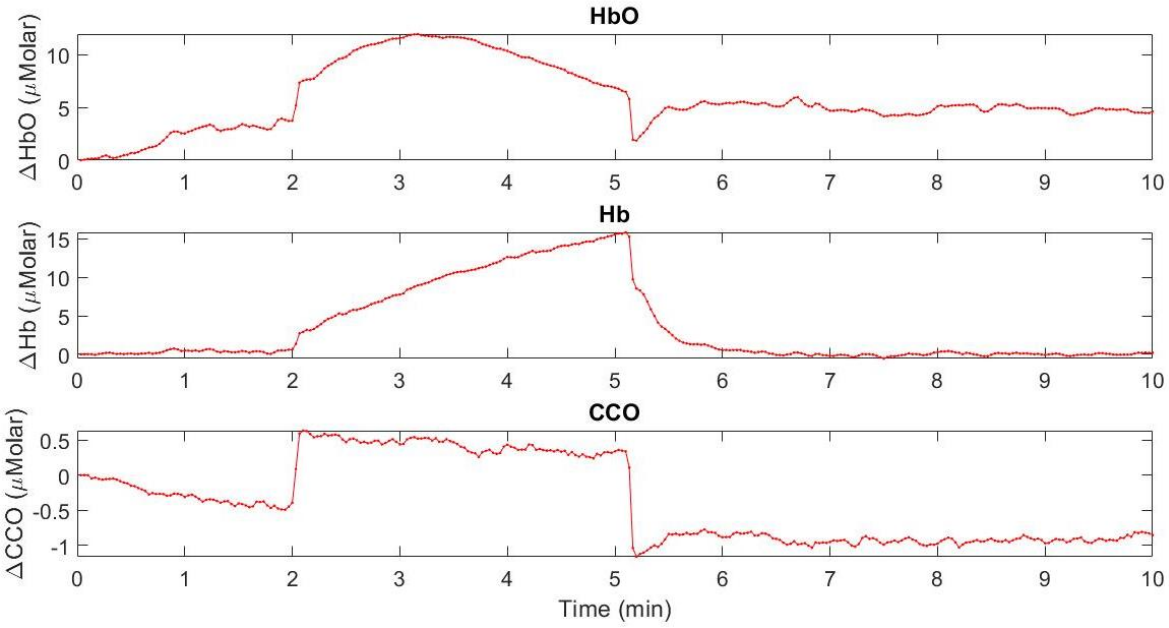

Figure 3-15: Subject 6's HbO, HHb, and CCO time series for the right forearm.

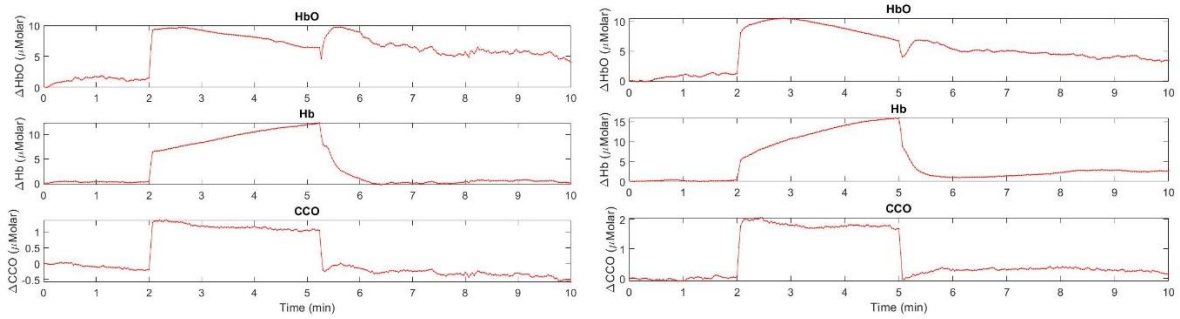

Figure 3-16: Subject 7's HbO, HHb, and CCO time series for the left forearm (left) and right forearm (right).

3.4 Discussion

As mentioned in the Introduction, vascular occlusion tests are common practice in the field of near-infrared spectroscopy. The temporal curves of HbO and Hb before, during, and after the forearm occlusion as shown in Figures 3-10 to 3-16 are typical results in numerous reports. These curves show that under arterial occlusion, changes in HbO and Hb concentrations would decrease and increase, respectively, owing to the lack of oxygen supplies, as expected. However, few studies have reported changes of oxidized CCO concentration in response to arterial occlusion. Theoretically, the concentration of oxidized CCO should decrease if no oxygen is available. This expectation was observed in several participants' data after a prompt rise resulting from the initial veinous occlusion. However, the overall results across the seven participants were somewhat inconsistent, which could be attributed to the small sample size and exploratory experiments. Further investigation with a larger sample size and consistent experimental protocol is currently underway to better understand the physiology of mitochondrial or metabolic responses to a lack of blood oxygen.

Moreover, WTC is a new approach for analyzing and quantifying hemodynamic and metabolic coupling in response to arterial occlusions. These initial results are intriguing and may reveal new findings. For subjects 1-5, the occlusion period was 5 min after the 2-min baseline period. As seen below, during the baseline and the initial occlusion phase, HbO and CCO are strongly in-phase coupled across all three ISO frequencies (endogenic: 0.005-0.02 Hz; neurogenic: 0.02-0.04 Hz; myogenic: 0.04-0.2 Hz) as marked by three horizontal lines in the following figure, while the coherence in the endogenic band is limited due to COI. It is clear that the decoupling between the two started in the endogenic oscillation, continued, and expanded gradually into the other two oscillation (neurogenic and myogenic) bands, as seen by the blue curvy band across the occlusion period (2-7 min). After a short period of decoupling between

HbO and CCO during arterial occlusion, the coupling was restored with strong anti-phase coupling across the three ISO frequencies. This anti-phase coupling remained for 1 min or longer after the occlusion phase. This set of in-phase coupling, decoupling, and anti-phase recoupling features was observed consistently in most of the WTC maps shown in Figures 3-3, 3-7, and 3-9.

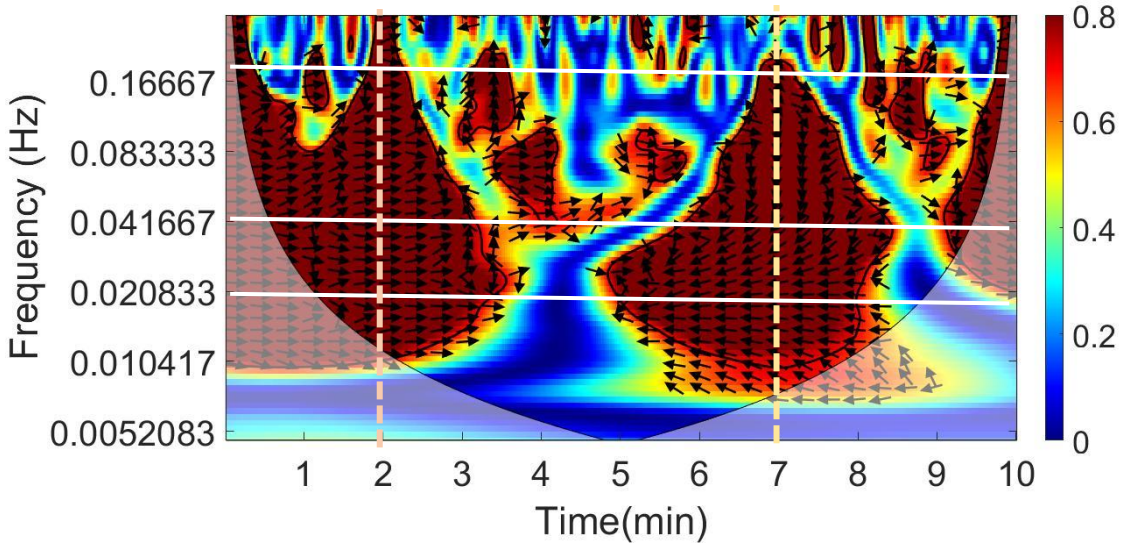

Figure 3-17: The WTC heat map from figure 3-1 showing the start of occlusion (2 min mark) and the end of occlusion (7 min mark), as well as the three ISO bands on the y-axis.

The three features of in-phase coupling, decoupling, and anti-phase recoupling features are first-time seen, which may reveal much underlying physiology of metabolic-vascular coupling in the oxygen-deficient environment or serve features/markers for vascular health. Further understanding of the data and confirmation of the findings are beyond my role in this exploratory study. All the results presented in this subsection will serve as excellent preliminary data for further investigations.

References

1. Ginglen JG, Butki N. Necrotizing Enterocolitis. [Updated 2022 Aug 8]. In: StatPearls [Internet]. Treasure Island (FL): StatPearls Publishing; 2022 Jan-. Available from: https://www.ncbi.nlm.nih.gov/books/NBK513357/

2. Ramani M, Ambalavanan N. Feeding practices and necrotizing enterocolitis. Clin Perinatol. 2013 Mar;40(1):1-10. doi: 10.1016/j.clp.2012.12.001. Epub 2013 Jan 17. PMID: 23415260; PMCID: PMC3576724.

3. Chernikova, D.A., Madan, J.C., Housman, M.L. *et al.* The premature infant gut microbiome during the first 6 weeks of life differs based on gestational maturity at birth. *Pediatr Res* **84**, 71–79 (2018). https://doi.org/10.1038/s41390-018-0022-z

4. Indrio F, Neu J, Pettoello-Mantovani M, Marchese F, Martini S, Salatto A, Aceti A. Development of the Gastrointestinal Tract in Newborns as a Challenge for an Appropriate Nutrition: A Narrative Review. Nutrients. 2022 Mar 28;14(7):1405. doi: 10.3390/nu14071405. PMID: 35406018; PMCID: PMC9002905.

5. Yin J, Chen JD. Electrogastrography: methodology, validation and applications. J Neurogastroenterol Motil. 2013 Jan;19(1):5-17. doi: 10.5056/jnm.2013.19.1.5. Epub 2013 Jan 8. PMID: 23350042; PMCID: PMC3548127.

6. J. D. Chen, R. W. Schirmer Bd Fau - McCallum, and R. W. McCallum, "Serosal and cutaneous recordings of gastric myoelectrical activity in patients with gastroparesis," Am J Physiol 0002- 9513 (Print)), 266(261 Pt 261):G290-G298 (1994).

7. Chaudhari, A., Wang, X., Roblyer, L. *et al.* Frequency-specific electrogastrography as a non-invasive tool to measure gastrointestinal maturity in preterm infants. *Sci Rep* **12**, 20728 (2022). https://doi.org/10.1038/s41598-022-24110-y

8. Popović, N.B., Miljković, N. and Popović, M.B., 2019. Simple gastric motility assessment method with a single-channel electrogastrogram. *Biomedical Engineering/Biomedizinische Technik*, *64*(2), pp.177-185, doi: 10.1515/bmt-2017-0218.

9. Popović, N.B., Miljković, N. and Popović, M.B., 2020. Three-channel surface electrogastrogram (EGG) dataset recorded during fasting and post-prandial states in 20 healthy individuals [Data set]. *Zenodo*, doi: 10.5281/zenodo.3730617.

10. Lee, J.-H., Jang, Y.-E., Song, I.-K., Kim, E.-H., Kim, H.-S., & Kim, J.-T. (2018). Near-infrared spectroscopy and vascular occlusion test for predicting clinical outcome in pediatric cardiac patients. *Pediatric Critical Care Medicine, 19*(1), 32–39. https://doi.org/10.1097/pcc.0000000000001386

11. Veal, J. R., & McCord, W. M. (1939). Blood oxygen changes following intermittent venous occlusion. *American Heart Journal*, *17*(4), 401–405. https://doi.org/10.1016/s0002-8703(39)90589-2

12. Sadra Shahdadian, Xinlong Wang, Shu Kang, Caroline Carter, Akhil Chaudhari, Hanli Liu, Prefrontal cortical connectivity and coupling of infraslow oscillation in the resting human brain: a 2-channel broadband NIRS study, *Cerebral Cortex Communications*, Volume 3, Issue 3, 2022, tgac033, https://doi.org/10.1093/texcom/tgac033

13. Wang X, Tian F, Soni SS, Gonzalez-Lima F, Liu H. Interplay between up-regulation of cytochrome-c-oxidase and hemoglobin oxygenation induced by near-infrared laser. Sci Rep. 2016 Aug 3;6:30540. doi: 10.1038/srep30540. PMID: 27484673; PMCID: PMC4971496.

14. Aslak Grinsted (2023). Cross wavelet and wavelet coherence (https://github.com/grinsted/wavelet-coherence), GitHub. Retrieved March 27, 2023.

15. Arnsten AF. Stress signalling pathways that impair prefrontal cortex structure and function. Nat Rev Neurosci. 2009 Jun;10(6):410-22. doi: 10.1038/nrn2648. PMID: 19455173; PMCID: PMC2907136.

16. Herrmann MJ, Langer JB, Jacob C, Ehlis AC, Fallgatter AJ. Reduced prefrontal oxygenation in Alzheimer disease during verbal fluency tasks. Am J Geriatr Psychiatry. 2008 Feb;16(2):125-35. doi: 10.1097/JGP.0b013e3180cc1fbc. Epub 2007 Nov 12. PMID: 17998307.

17. *Alzheimer's disease facts and figures*. Alzheimer's Disease and Dementia. (n.d.). Retrieved April 4, 2023, from https://www.alz.org/alzheimers-dementia/facts-figures

18. Wang, X., Tian, F., Soni, S. S., Gonzalez-Lima, F., & Liu, H. (2016). Interplay between up-regulation of cytochrome-c-oxidase and hemoglobin oxygenation induced by near-infrared laser. *Scientific reports*, *6*(1), 1-10.

19. Kvernmo, H. D., A. Stefanovska, K. A. Kirkeboen, and K. Kvernebo. 1999. 'Oscillations in the human cutaneous blood perfusion signal modified by endothelium-dependent and endothelium-independent vasodilators', *Microvasc Res*, 57: 298-309.

20. Shahdadian, S., Wang, X., Kang, S., Carter, C., Chaudhari, A., & Liu, H. (2022). Prefrontal cortical connectivity and coupling of infraslow oscillation in the resting human brain: a 2-channel broadband NIRS study. *Cerebral Cortex Communications*, *3*(3), tgac033.

21. *Multi-taper method (MTM)*. Multi-Taper Method (MTM). (n.d.). Retrieved April 4, 2023, from https://dept.atmos.ucla.edu/tcd/multi-taper-method-mtm

22. *Slepian or DPSS window*. CCRMA. (n.d.). Retrieved April 4, 2023, from https://ccrma.stanford.edu/~jos/sasp/Slepian_DPSS_Window.html

23. Bastos AM, Schoffelen JM. A Tutorial Review of Functional Connectivity Analysis Methods and Their Interpretational Pitfalls. Front Syst Neurosci. 2016 Jan 8;9:175. doi: 10.3389/fnsys.2015.00175. PMID: 26778976; PMCID: PMC4705224.

24. Dohi, Y., Kojima, M., Sato, K. *et al.* Age-Related Changes in Vascular Smooth Muscle and Endothelium. *Drugs & Aging* **7**, 278–291 (1995). https://doi.org/10.2165/00002512-199507040-00003

Appendix: Codes used in Chapter 1

Numbers have been added to the flowchart from figure 1-3 to show which of the following codes correspond to each step of data processing.

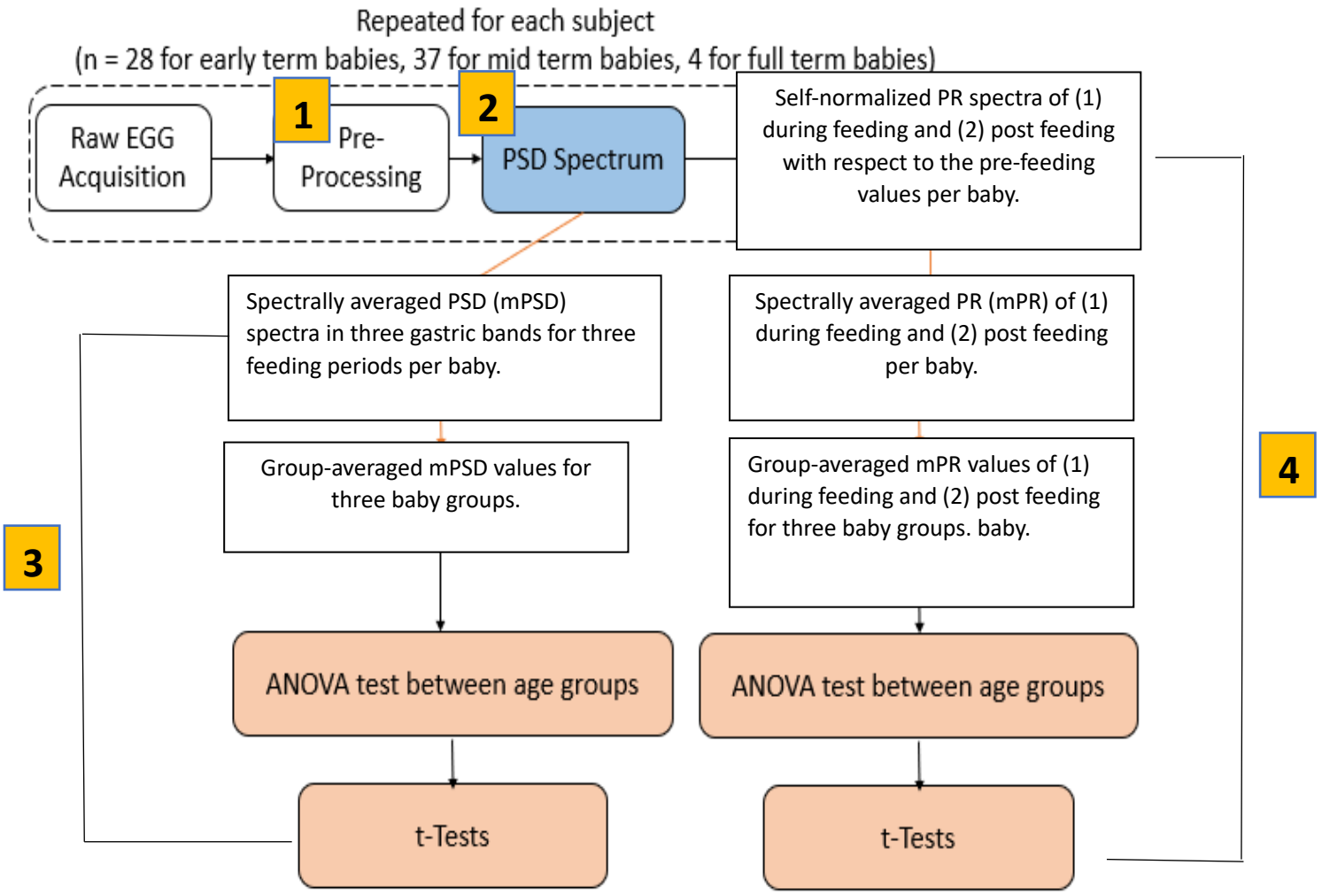

1. Data Pre-processing (egg_generate_mat_file.m):

```
clear all;      clc;
sub_no = 'POOH085';     parent_folder = 'F:\Fall 2022 EGG PSD Practice';
%folder with all subjects
% egg_folder_end_name = '_2-15';
egg_fd = 'F:\Fall 2022 EGG PSD Practice\SUBS 76-88\POOH085\EGG';  %folder
with subject's EGG data
nirs_fd = 'F:\Fall 2022 EGG PSD Practice\SUBS 76-88\POOH085\NIRS';
%folder with subject's NIRS data
```

```
file_name_egg = 'POOH085-9 (GI_Devel_Study_Temp_03262018_v4).txt';  %name of
EGG file for week
file_name_nirs = '220216N_POOH085-9.R22';                          %name of
NIRS file for week

result_mat_file = 'EGG_nirs_data_SUB85-9.mat'; %what you want to name results
file: EGG_nirs_data_SUB(number)-(week).mat
result_directory = 'F:\Fall 2022 EGG PSD Practice\SUBS 76-
88\POOH085\results'; %where you want to save results

addpath 'F:\Fall 2022 EGG PSD Practice\SUBS 76-88\POOH085\EGG';   %add path
to subject's EGG data
addpath 'F:\Fall 2022 EGG PSD Practice\SUBS 76-88\POOH085\NIRS';  %add path
to subject's NIRS data
% num_of_files_need = 8;  %number of files in NIRS folder
%% Calculate common_read, time_var, numer_data, temp45 - find 121 mark

%Load NIRS data
% nirs_data = importdata(file_name_nirs);
% nirs_data2 = split(nirs_data);
% numer_data = str2double(nirs_data2); clear nirs_data clear
% data_nirs = nirs_data2;
% z = data_nirs(:,3);     time_var = str2double(split(z,':')); clear
nirs_data2
%



%% Load data from 1 EGG file & save it

        %if data is in a .txt file:
        Data = importdata(file_name_egg);           clear file_name_egg
        EGG = Data.data(2:end,2);
        EGG_time_sec = Data.data(2:end,1)*60*60;EGG_time_sec(:,3) =
Data.data(2:end,1);  clear Data

        %if data is in another format
%         egg_data = importdata(file_name_egg);
%         egg_data2 = split(egg_data);
%         numer_data_egg = str2double(egg_data2); clear nirs_data clear
%         data_egg = egg_data2;
%         z_egg = data_egg(:,3);    clear egg_data2

        cd(parent_folder); % change to where you will store the function
being used
        common_read = []; temp45 = 1; %these variables aren't used in
eeg_fnirsv3, so just make them up

[com_data,pl_data,time_calc]=eeg_fnirsv3(time_var,numer_data,EGG,EGG_time_sec
,temp45,common_read);

        clear com_data data_nirs data_nirs EGG  numer_data

        nirs_121_a{temp45} = pl_data.a_121_data;
        nirs_121_c{temp45} = pl_data.c_121_data;
```

```
        nirs_121_time{temp45} = pl_data.nirs_121_time;
        EGG_121_time{temp45}=pl_data.EGG_121_time;
        temp_EGG = pl_data.EGG_121_data;
        fs = 2000;
dataIn = double(temp_EGG);



%% Pre-process EGG data

%Downsample to 500 Hz
dsr=round(fs/500);
temp45 = 1;
EGG_121_data{temp45} =( downsample(dataIn.', dsr) ).'; % data in in space
time but downsample.m wants time space
fs = 500; % change if does not need to downsample

kk=1;
%Detrending
dataIn1 = EGG_121_data{kk};
t1 = linspace(0,EGG_121_time{kk}(end,1),length(EGG_121_data{kk}));
p = polyfit(t1',dataIn1,3);
trend = polyval(p,t1);

dataIn0 = dataIn1 - trend';

%Filtering
fl=0.37; % 1 Hz cutoff
[b,a]=butter(2,fl/(fs/2) ,'low');
% figure(3); freqz(b,a,[],fs); % verify that your high pass filter is correct
dataOut=filtfilt(b,a,dataIn0');
dataOut_final{kk} = dataOut';
EGG_121_data_final = dataOut_final{kk};
clear dataOut_final dataIn;

%% Save all relevant variables as .mat file

end_time_indx1 = 1; end_time_indx2 = 1;
start_time_indx1 = 1; start_time_indx2 = 1;
cd(result_directory);    %GO TO RESULTS DIRECTORY
save(result_mat_file,
'EGG_121_data_final','EGG_121_time','end_time_indx1','end_time_indx2','nirs_1
21_time','nirs_121_a','nirs_121_c','start_time_indx1','start_time_indx2');

%% Full spectrum PSD
figure;
fs_EGG = 500;
[EGG_pre1_psd freq_EGG_psd] =
pwelch(EGG_121_data_final,240*fs_EGG,0.5*240*fs_EGG,round(1000*fs_EGG),fs_EGG
);
cpm = freq_EGG_psd .* 60; %gastric spectrum: 0.5-9 cpm; 0.48 (9) - 9 (151)
(9-51)
loglog(freq_EGG_psd(9:151,:),EGG_pre1_psd(9:151));
xlabel('Frequency (Hz)'); ylabel('Power Spectral Density W/Hz'); title('Full
Recording');
```

```
hold on;
xticks([0 0.05 0.1 0.15]);
xticklabels({'0','0.05','0.1','0.15'});
ylim([0.03 10]); yticks([0.03 0.3 1 3]); yticklabels({'0.03','0.3','1','3'});
```

2. PSD Calculation (psd_calc_fixing_pwelch.m):

```
% Calculate PSD for one reading (of 1 subject)
clear all; close all;
sub_no = 46;    %change subject number
sub_read = 1;  %the specific reading/week
name_load = 'EGG_nirs_data_SUB46-1.mat';   %name of .mat file from
egg_generate_mat_file.m
results_fd = 'F:\Fall 2022 EGG PSD Practice\POOH046\results'; %change to
results fd
addpath(results_fd); %E:\Fall 2022 EGG PSD Practice\POOH021\results';

%% Load data
% Load timings for subject's subreading from FeedingTime.csv
timings_excel = importdata('FeedingTime.csv');
if(sub_no>=10)
    sub_no_line = strcat('POOH0',num2str(sub_no));  %subject index in excel
sheet
else
    sub_no_line = strcat('POOH00',num2str(sub_no));  %subject index in excel
sheet
end

read_no_line = strcat('week_',num2str(sub_read),'_arm_1');  %reading index in
excel sheet
line_no = find(strcmpi(timings_excel.textdata(:,1),sub_no_line));
read_no = find(strcmpi(timings_excel.textdata(:,2),read_no_line));
reading = find(read_no>=line_no(1,:),1); reading = read_no(reading,:);
timing_data = timings_excel.data(reading-1,:); %reading-1 bc excel sheet has
top row w/ descriptors
clear timings_excel line_no read_no reading sub_no_line read_no_line

load(name_load);clear end_time_indx1 end_time_indx2 start_time_indx1
start_time_indx2 name_load
clear nirs_121_time nirs_a_121 nirs_c_121
% change EGG_121_time to downsampled data
EGG_timings = EGG_121_time{1,1};
EGG_time =
linspace(EGG_timings(1,1),EGG_timings(end,1),size(EGG_121_data_final,1));
clear EGG_121_time
EGG_121_time = EGG_time';    clear EGG_time EGG_timings;
fs_EGG = size(EGG_121_data_final,1)/EGG_121_time(end,1);    %should be 500 Hz

% extract the feeding periods from the excel sheet
% col 4-5 feed 1 start-end;  col 8-9 feed 2 start-end
feed_time = [timing_data(1,4) timing_data(1,5) timing_data(1,8)
timing_data(1,9)]; clear timing_data
diff_f = feed_time(1,2)-feed_time(1,1);
```

```
%% Pwelch
EGG_121_data_final = EGG_121_data_final';
k=1; k1=1;
            % some conditions to make sure that data is in right format
            if diff_f~=0
                clear diff_f
                if feed_time(1,1)~=0
                    % extract time for feeding 1, pre, dur and post
                    tt.EGG_dur1 =
[max(find(EGG_121_time(:,1)<=feed_time(1,1)))
max(find(EGG_121_time(:,1)<=feed_time(1,2)))];
                    tt.EGG_pre1 = [1 tt.EGG_dur1(1,1)];

                    if isnan(feed_time(1,3))
                        tt.EGG_post1 = [tt.EGG_dur1(1,2)
max(find(EGG_121_time(:,1)<=(feed_time(1,2)+30*60)))]; % 30 min as post 1
                        tt.EGG_dur2 = [NaN NaN];  tt.EGG_pre2 = [NaN NaN];
tt.EGG_post2 = [NaN NaN];
                    else
                        tt.EGG_dur2 =
[max(find(EGG_121_time(:,1)<=feed_time(1,3)))
max(find(EGG_121_time(:,1)<=feed_time(1,4)))];
                        EGG_mid = tt.EGG_dur2(1,1) - tt.EGG_dur1(1,2);
                        tt.EGG_post1 = [tt.EGG_dur1(1,2)
tt.EGG_dur1(1,2)+(EGG_mid/2)];
                        tt.EGG_pre2 = [tt.EGG_dur2(1,1)-(EGG_mid/2)
tt.EGG_dur2(1,1)]; clear EGG_mid
                        tt.EGG_post2 = [tt.EGG_dur2(1,2)
size(EGG_121_time,1)];
                    end
                    clear time_tt_var feed_time

                    % extract data from the whole EEG data
                    f_data.EGG_pre1 =
EGG_121_data_final(1,tt.EGG_pre1(1,1):tt.EGG_pre1(1,2));
                    f_data.EGG_dur1 =
EGG_121_data_final(1,tt.EGG_dur1(1,1):tt.EGG_dur1(1,2));
                    f_data.EGG_post1 =
EGG_121_data_final(1,tt.EGG_post1(1,1):tt.EGG_post1(1,2));
                    if length(f_data.EGG_pre1)>=30 % check if pre feeding is
> 30 min
                        if length(f_data.EGG_dur1)>=30 % check if dur feeding
is > 30 min
                            if length(f_data.EGG_post1)>=30 % check if post
feeding is > 30 min
                                % run pwelch to get the PSD, 240sec in 4min
                                [EGG_pre1_psd freq_EGG_psd] =
pwelch(f_data.EGG_pre1,240*fs_EGG,0.5*240*fs_EGG,round(1000*fs_EGG),fs_EGG);
                                [EGG_dur1_psd freq_EGG_psd] =
pwelch(f_data.EGG_dur1,240*fs_EGG,0.5*240*fs_EGG,round(1000*fs_EGG),fs_EGG);
                                [EGG_post1_psd freq_EGG_psd] =
pwelch(f_data.EGG_post1,240*fs_EGG,0.5*240*fs_EGG,round(1000*fs_EGG),fs_EGG);

                                k=k+1;
                            end
                        end
```

```
                    end

                    if ~isnan(tt.EGG_dur2(1,1))
                        f_data.EGG_pre2 =
EGG_121_data_final(1,tt.EGG_pre2(1,1):tt.EGG_pre2(1,2));
                        f_data.EGG_dur2 =
EGG_121_data_final(1,tt.EGG_dur2(1,1):tt.EGG_dur2(1,2));
                        f_data.EGG_post2 =
EGG_121_data_final(1,tt.EGG_post2(1,1):tt.EGG_post2(1,2));
                        if length(f_data.EGG_pre2)>=30 % check if pre feeding
is > 30 min
                            if length(f_data.EGG_dur2)>=30 % check if dur
feeding is > 30 min
                                if length(f_data.EGG_post2)>=30 % check if
post feeding is > 30 min
                                    % run pwelch to get the PSD
                                    [EGG_pre2_psd freq_EGG_psd] =
pwelch(f_data.EGG_pre2,240*fs_EGG,0.5*240*fs_EGG,round(1000*fs_EGG),fs_EGG);
                                    [EGG_dur2_psd freq_EGG_psd] =
pwelch(f_data.EGG_dur2,240*fs_EGG,0.5*240*fs_EGG,round(1000*fs_EGG),fs_EGG);
                                    [EGG_post2_psd freq_EGG_psd] =
pwelch(f_data.EGG_post2,240*fs_EGG,0.5*240*fs_EGG,round(1000*fs_EGG),fs_EGG);
                                    k1=k1+1;
                                end
                            end
                        end
                        clear f_data EGG_121_time fs_EGG name_load
                    end
                    clear tt nirs_a_121 nirs_c_121 EGG_121_data_final f_data
EGG_121_time fs_EGG name_load
                else
                    clear EGG_121_data_final EGG_121_time feed_time fs_EGG
fs_nirs name_load nirs_121_time nirs_a_121 nirs_c_121
                end
            end

            cd(results_fd);
            savename = strcat('EGG_PSD_results_SUB',num2str(sub_no),'-
',num2str(sub_read),'NEW','.mat');
%             CHECK FEEDING FILE - if no feed1/feed2, don't save those
variables
           if(exist('EGG_pre2_psd'))

save(savename,'freq_EGG_psd','EGG_dur1_psd','EGG_dur2_psd','EGG_post1_psd','E
GG_post2_psd','EGG_pre1_psd','EGG_pre2_psd');
           else

save(savename,'freq_EGG_psd','EGG_dur1_psd','EGG_post1_psd','EGG_pre1_psd');
           end
```

3. mPSD Calculation (mean_PSD_ver_akhil.m):

```
% Early: <29 wks, Mid: 29-33 wks, Term: >= 37 wks
% NOTE: Separate babies into 3 folders for the 3 age ranges before running
% These folders should ONLY have the PSD results.
```

```
clear all; close all;
all_subs_fd = 'F:\Fall 2022 EGG PSD Practice\All PSD Data\'; %folder with all
babies' PSD. KEEP SLASH AT END
age_range = ["early","mid","term"]; %replace with 'early', 'mid', or 'term'

%% Create arrays with data from all subjects
for mm=1:length(age_range)
age_fd = strcat(all_subs_fd, age_range(mm));
cd(age_fd); %change to folder for specific age range results

list_results = dir(age_fd);
num_results = length(list_results) - 2; %subtract parent folder & subfolder
(. & ..) to get number of PSD files

for i=3:length(list_results)  %start at 3 so you skip . & ..
    fname = list_results(i).name;
    load(fname);
    if(exist('EGG_pre1_psd'))
        EGG_pre1_psd_all(i-2,:) = EGG_pre1_psd; %i-2 gets rid of parent
folder & subfolder name
    end
    if(exist('EGG_dur1_psd'))
        EGG_dur1_psd_all(i-2,:) = EGG_dur1_psd;
    end
    if(exist('EGG_post1_psd'))
        EGG_post1_psd_all(i-2,:) = EGG_post1_psd;
    end
    if(exist('EGG_pre2_psd'))
        EGG_pre2_psd_all(i-2,:) = EGG_pre2_psd;
    end
    if(exist('EGG_dur2_psd'))
        EGG_dur2_psd_all(i-2,:) = EGG_dur2_psd;
    end
    if(exist('EGG_post2_psd'))
        EGG_post2_psd_all(i-2,:) = EGG_post2_psd;
    end
end
clear EGG_pre1_psd EGG_dur1_psd EGG_post1_psd EGG_pre2_psd EGG_dur2_psd
EGG_post2_psd i EGG_dur1_psd
%% Average & calculate STE PSD for each period
% Averaging:
EGG_pre1_avg = mean(EGG_pre1_psd_all,1);
EGG_dur1_avg = mean(EGG_dur1_psd_all,1);
EGG_post1_avg = mean(EGG_post1_psd_all,1);
EGG_pre2_avg = mean(EGG_pre2_psd_all,1);
EGG_dur2_avg = mean(EGG_dur2_psd_all,1);
EGG_post2_avg = mean(EGG_post2_psd_all,1);

EGG_pre1_STE = std(EGG_pre1_psd_all,1)/sqrt(length(num_results));
EGG_dur1_STE = std(EGG_dur1_psd_all,1)/sqrt(length(num_results));
EGG_post1_STE = std(EGG_post1_psd_all,1)/sqrt(length(num_results));
EGG_pre2_STE = std(EGG_pre2_psd_all,1)/sqrt(length(num_results));
EGG_dur2_STE = std(EGG_dur2_psd_all,1)/sqrt(length(num_results));
EGG_post2_STE = std(EGG_post2_psd_all,1)/sqrt(length(num_results));
```

```
% AVERAGING FEEDING PERIODS 1 & 2:
EGG_pre = [EGG_pre1_psd_all; EGG_pre2_psd_all]; %combine PSDs: # of subjects
x [feed1 feed2]
EGG_dur = [EGG_dur1_psd_all; EGG_dur2_psd_all];
EGG_post = [EGG_post1_psd_all; EGG_post2_psd_all];

EGG_pre_avg = mean(EGG_pre); EGG_pre_STE =
std(EGG_pre,0,1)/sqrt(length(EGG_pre(:,1)));
EGG_dur_avg = mean(EGG_dur); EGG_dur_STE =
std(EGG_dur,0,1)/sqrt(length(EGG_dur(:,1)));
EGG_post_avg = mean(EGG_post); EGG_post_STE =
std(EGG_post,0,1)/sqrt(length(EGG_post(:,1)));

% For ANOVA:
for i=1:num_results
    EGG_pre_temp = [EGG_pre1_psd_all(i,:)' EGG_pre2_psd_all(i,:)'];
    EGG_pre_st(i,:,:) = mean(EGG_pre_temp,2);
    EGG_dur_temp = [EGG_dur1_psd_all(i,:)' EGG_dur2_psd_all(i,:)'];
    EGG_dur_st(i,:,:) = mean(EGG_dur_temp,2);
    EGG_post_temp = [EGG_post1_psd_all(i,:)' EGG_post2_psd_all(i,:)'];
    EGG_post_st(i,:,:) = mean(EGG_post_temp,2);
end
clear EGG_pre_temp EGG_dur_temp EGG_post_temp;
clear EGG_pre1_psd_all EGG_pre2_psd_all EGG_dur1_psd_all EGG_dur2_psd_all
EGG_post1_psd_all EGG_post2_psd_all;

% ANOVA:
for i=1:num_results  %start at 3 so you skip . & ..
    if(i==1)
        b_pre(:,:) = EGG_pre_st(i,10:34)';
        n_pre(:,:) = EGG_pre_st(i,35:67)';
        t_pre(:,:) = EGG_pre_st(i,68:151)';

        b_dur(:,:) = EGG_dur_st(i,10:34)';
        n_dur(:,:) = EGG_dur_st(i,35:67)';
        t_dur(:,:) = EGG_dur_st(i,68:151)';

        b_post(:,:) = EGG_post_st(i,10:34)';
        n_post(:,:) = EGG_post_st(i,35:67)';
        t_post(:,:) = EGG_post_st(i,68:151)';
    else
        b_pre = cat(1,b_pre,EGG_pre_st(i,10:34)');
        n_pre = cat(1,n_pre,EGG_pre_st(i,35:67)');
        t_pre = cat(1,t_pre,EGG_pre_st(i,68:151)');

        b_dur = cat(1,b_dur,EGG_dur_st(i,10:34)');
        n_dur = cat(1,n_dur,EGG_dur_st(i,35:67)');
        t_dur = cat(1,t_dur,EGG_dur_st(i,68:151)');

        b_post = cat(1,b_post,EGG_post_st(i,10:34)');
        n_post = cat(1,n_post,EGG_post_st(i,35:67)');
        t_post = cat(1,t_post,EGG_post_st(i,68:151)');
    end
end
clear b_pre b_dur b_post n_pre n_dur n_post t_pre t_dur t_post;
```

```
% Saving averages for ANOVA
% all_brady_pre(mm,:) = EGG_pre_avg(10:34);
% all_normo_pre(mm,:) = EGG_pre_avg(35:67);
% all_tachy_pre(mm,:) = EGG_pre_avg(68:151);
%
% all_brady_dur(mm,:) = EGG_dur_avg(10:34);
% all_normo_dur(mm,:) = EGG_dur_avg(35:67);
% all_tachy_dur(mm,:) = EGG_dur_avg(68:151);
%
% all_brady_post(mm,:) = EGG_post_avg(10:34);
% all_normo_post(mm,:) = EGG_post_avg(35:67);
% all_tachy_post(mm,:) = EGG_post_avg(68:151);

% Calculate mean PSD
mPSD_pre_brady = mean(EGG_pre_avg(10:34)); mPSD_pre_brady_STE =
std(EGG_pre_avg(10:34))/sqrt(length(EGG_pre_avg(10:34)));
mPSD_pre_normo = mean(EGG_pre_avg(35:67)); mPSD_pre_normo_STE =
std(EGG_pre_avg(43:60))/sqrt(length(EGG_pre_avg(35:67)));
mPSD_pre_tachy = mean(EGG_pre_avg(68:151));mPSD_pre_tachy_STE =
std(EGG_pre_avg(68:151))/sqrt(length(EGG_pre_avg(68:151)));

mPSD_dur_brady = mean(EGG_dur_avg(10:34)); mPSD_dur_brady_STE =
std(EGG_dur_avg(10:34))/sqrt(length(EGG_pre_avg(10:34)));
mPSD_dur_normo = mean(EGG_dur_avg(35:67)); mPSD_dur_normo_STE =
std(EGG_dur_avg(43:60))/sqrt(length(EGG_pre_avg(35:67)));
mPSD_dur_tachy = mean(EGG_dur_avg(68:151)); mPSD_dur_tachy_STE =
std(EGG_dur_avg(68:151))/sqrt(length(EGG_pre_avg(68:151)));

mPSD_post_brady = mean(EGG_post_avg(10:34)); mPSD_post_brady_STE =
std(EGG_post_avg(10:34))/sqrt(length(EGG_pre_avg(10:34)));
mPSD_post_normo = mean(EGG_post_avg(35:67)); mPSD_post_normo_STE =
std(EGG_post_avg(43:60))/sqrt(length(EGG_pre_avg(35:67)));
mPSD_post_tachy = mean(EGG_post_avg(68:151)); mPSD_post_tachy_STE =
std(EGG_post_avg(68:151))/sqrt(length(EGG_pre_avg(68:151)));

brady = [mPSD_pre_brady mPSD_dur_brady  mPSD_post_brady];
normo = [mPSD_pre_normo mPSD_dur_normo  mPSD_post_normo];
tachy = [mPSD_pre_tachy mPSD_dur_tachy  mPSD_post_tachy];

brady_err = [mPSD_pre_brady_STE mPSD_dur_brady_STE  mPSD_post_brady_STE];
normo_err = [mPSD_pre_normo_STE mPSD_dur_normo_STE  mPSD_post_normo_STE];
tachy_err = [mPSD_pre_tachy_STE mPSD_dur_tachy_STE  mPSD_post_tachy_STE];

all_bands(mm,:,:) = [brady; normo; tachy];
all_err(mm,:,:) = [brady_err; normo_err; tachy_err];
% clear brady normo tachy brady_err normo_err tachy_err EGG_pre_avg
EGG_dur_avg EGG_post_avg;

end
%% for t-tests
% Bradygastria, pre:
% [h_brady_pre_earlymid, p_brady_pre_earlymid] =
ttest(all_brady_pre(1,:),all_brady_pre(2,:));
% [h_brady_pre_midterm, p_brady_pre_midterm] =
ttest(all_brady_pre(2,:),all_brady_pre(3,:));
```

```
% [h_brady_pre_earlyterm, p_brady_pre_earlyterm]=
ttest(all_brady_pre(1,:),all_brady_pre(3,:));
%
% % Bradygastria, dur:
% [h_brady_dur_earlymid, p_brady_dur_earlymid] =
ttest(all_brady_dur(1,:),all_brady_dur(2,:));
% [h_brady_dur_midterm, p_brady_dur_midterm] =
ttest(all_brady_dur(2,:),all_brady_dur(3,:));
% [h_brady_dur_earlyterm, p_brady_dur_earlyterm]=
ttest(all_brady_dur(1,:),all_brady_dur(3,:));
%
% % Bradygastria, post:
% [h_brady_post_earlymid, p_brady_post_earlymid] =
ttest(all_brady_post(1,:),all_brady_post(2,:));
% [h_brady_post_midterm, p_brady_post_midterm] =
ttest(all_brady_post(2,:),all_brady_post(3,:));
% [h_brady_post_earlyterm, p_brady_post_earlyterm]=
ttest(all_brady_post(1,:),all_brady_post(3,:));
%
% % Normogastria, pre:
% [h_normo_pre_earlymid, p_normo_pre_earlymid] =
ttest(all_normo_pre(1,:),all_normo_pre(2,:));
% [h_normo_pre_midterm, p_normo_pre_midterm] =
ttest(all_normo_pre(2,:),all_normo_pre(3,:));
% [h_normo_pre_earlyterm, p_normo_pre_earlyterm]=
ttest(all_normo_pre(1,:),all_normo_pre(3,:));
%
% % Normogastria, dur:
% [h_normo_dur_earlymid, p_normo_dur_earlymid] =
ttest(all_normo_dur(1,:),all_normo_dur(2,:));
% [h_normo_dur_midterm, p_normo_dur_midterm] =
ttest(all_normo_dur(2,:),all_normo_dur(3,:));
% [h_normo_dur_earlyterm, p_normo_dur_earlyterm]=
ttest(all_normo_dur(1,:),all_normo_dur(3,:));
%
% % Normogastria, post:
% [h_normo_post_earlymid, p_normo_post_earlymid] =
ttest(all_normo_post(1,:),all_normo_post(2,:));
% [h_normo_post_midterm, p_normo_post_midterm] =
ttest(all_normo_post(2,:),all_normo_post(3,:));
% [h_normo_post_earlyterm, p_normo_post_earlyterm]=
ttest(all_normo_post(1,:),all_normo_post(3,:));
%
% % Tachygastria, pre:
% [h_tachy_pre_earlymid, p_tachy_pre_earlymid] =
ttest(all_tachy_pre(1,:),all_tachy_pre(2,:));
% [h_tachy_pre_midterm, p_tachy_pre_midterm] =
ttest(all_tachy_pre(2,:),all_tachy_pre(3,:));
% [h_tachy_pre_earlyterm, p_tachy_pre_earlyterm]=
ttest(all_tachy_pre(1,:),all_tachy_pre(3,:));
%
% % Bradygastria, dur:
% [h_tachy_dur_earlymid, p_tachy_dur_earlymid] =
ttest(all_tachy_dur(1,:),all_tachy_dur(2,:));
% [h_tachy_dur_midterm, p_tachy_dur_midterm] =
ttest(all_tachy_dur(2,:),all_tachy_dur(3,:));
```

```
% [h_tachy_dur_earlyterm, p_tachy_dur_earlyterm]=
ttest(all_tachy_dur(1,:),all_tachy_dur(3,:));
%
% % Bradygastria, post:
% [h_tachy_post_earlymid, p_tachy_post_earlymid] =
ttest(all_tachy_post(1,:),all_tachy_post(2,:));
% [h_tachy_post_midterm, p_tachy_post_midterm] =
ttest(all_tachy_post(2,:),all_tachy_post(3,:));
% [h_tachy_post_earlyterm, p_tachy_post_earlyterm]=
ttest(all_tachy_post(1,:),all_tachy_post(3,:));
%



%% Plot 3 figures for 3 freq bands (brady/normo/tachy)
% Plot for bradygastria
figure;
M = categorical({'Pre','During','Post'});
M = reordercats(M,{'Pre','During','Post'});
brady(1,:) = all_bands(:,1,1); brady(2,:) = all_bands(:,1,2); brady(3,:) =
all_bands(:,1,3);
brady_err(1,:) = all_err(:,1,1); brady_err(2,:) = all_err(:,1,1);
brady_err(3,:) = all_err(:,1,1);

h = bar(M,brady);% h will have 3 handles, one for each color of bars

hBar = bar(brady, 0.8);                                                    %
Return 'bar' Handle
set(hBar(:,1),'FaceColor',"#4DBEEE"); set(hBar(:,2),'FaceColor',"#D95319");
set(hBar(:,3),'FaceColor',"#77AC30");
for k1 = 1:size(brady,2)
    ctr(k1,:) = bsxfun(@plus, hBar(k1).XData, hBar(k1).XOffset');       %
Note: 'XOffset' Is An Undocumented Feature, This Selects The 'bar' Centres
    ydt(k1,:) = hBar(k1).YData;                                            %
Individual Bar Heights
end
hold on
errorbar(ctr, ydt, brady_err, '.r')                                        %
Plot Error Bars
hold off
set(gca,'XTickLabel',M)
ax = gca;
ax.FontSize = 16;
legend('Early','Mid','Term');
ylabel('Power Spectral Density \muV^2/Hz');
ylim([0 5.5]); yticks([0:1:5]); yticklabels({'0' '1' '2' '3' '4' '5'});
title("Bradygastria mPSD");
a = get(gca,'XTickLabel');
set(gca,'XTickLabel',a,'fontsize',12,'FontWeight','bold')
ax = gca;
ax.FontSize = 16;


% Plot for normogastria
figure;
```

```
M = categorical({'Pre','During','Post'});
M = reordercats(M,{'Pre','During','Post'});
normo(1,:) = all_bands(:,2,1); normo(2,:) = all_bands(:,2,2); normo(3,:) =
all_bands(:,2,3);
normo_err(1,:) = all_err(:,2,1); normo_err(2,:) = all_err(:,2,1);
normo_err(3,:) = all_err(:,2,1);

h = bar(M,normo);% h will have 3 handles, one for each color of bars

hBar = bar(normo, 0.8);                                                    %
Return 'bar' Handle
set(hBar(:,1),'FaceColor',"#4DBEEE"); set(hBar(:,2),'FaceColor',"#D95319");
set(hBar(:,3),'FaceColor',"#77AC30");
for k1 = 1:size(normo,2)
    ctr(k1,:) = bsxfun(@plus, hBar(k1).XData, hBar(k1).XOffset');       %
Note: 'XOffset' Is An Undocumented Feature, This Selects The 'bar' Centres
    ydt(k1,:) = hBar(k1).YData;                                            %
Individual Bar Heights
end
hold on
errorbar(ctr, ydt, normo_err, '.r')                                        %
Plot Error Bars
hold off
set(gca,'XTickLabel',M)
ax = gca;
ax.FontSize = 16;
legend('Early','Mid','Term');
ylabel('Power Spectral Density \muV^2/Hz');
ylim([0 1.6]); yticks([0:0.4:1.6]); yticklabels({'0' '0.4' '0.8' '1.2'
'1.6'});
title("Normogastria mPSD");
a = get(gca,'XTickLabel');
set(gca,'XTickLabel',a,'fontsize',12,'FontWeight','bold')
ax = gca;
ax.FontSize = 16;

% Plot for tachygastria
figure;
M = categorical({'Pre','During','Post'});
M = reordercats(M,{'Pre','During','Post'});
tachy(1,:) = all_bands(:,3,1); tachy(2,:) = all_bands(:,3,2); tachy(3,:) =
all_bands(:,3,3);
tachy_err(1,:) = all_err(:,3,1); tachy_err(2,:) = all_err(:,3,1);
tachy_err(3,:) = all_err(:,3,1);

h = bar(M,tachy);% h will have 3 handles, one for each color of bars

hBar = bar(tachy, 0.8);                                                    %
Return 'bar' Handle
set(hBar(:,1),'FaceColor',"#4DBEEE"); set(hBar(:,2),'FaceColor',"#D95319");
set(hBar(:,3),'FaceColor',"#77AC30");
for k1 = 1:size(tachy,2)
    ctr(k1,:) = bsxfun(@plus, hBar(k1).XData, hBar(k1).XOffset');       %
Note: 'XOffset' Is An Undocumented Feature, This Selects The 'bar' Centres
    ydt(k1,:) = hBar(k1).YData;                                            %
Individual Bar Heights
```

```
end
hold on
errorbar(ctr, ydt, tachy_err, '.r')                                    %
Plot Error Bars
hold off
set(gca,'XTickLabel',M)
ax = gca;
ax.FontSize = 16;
legend('Early','Mid','Term');
ylabel('Power Spectral Density \muV^2/Hz');
ylim([0 0.45]); yticks([0:0.1:0.4]); yticklabels({'0' '0.1' '0.2' '0.3'
'0.4'});
title("Tachygastria mPSD");
a = get(gca,'XTickLabel');
set(gca,'XTickLabel',a,'fontsize',12,'FontWeight','bold')
ax = gca;
ax.FontSize = 16;
```

4. Power Ratio & mPR Calculation (power_ratio_all_ages.m):

```
% Mean power ratio curves for all ages by taking ratio of each subject, THEN
averaging

clear all; close all;

all_subs_fd = 'F:\Fall 2022 EGG PSD Practice\All PSD Data\feeding
intolerance\'; %folder with all babies' PSD. KEEP SLASH AT END
age_range = ["DFI","PFI","NFI"]; %or replace with 'early', 'mid', or 'term'



for z=1:length(age_range)
%% Create arrays with data from all subjects
age_fd = strcat(all_subs_fd, age_range(z));
cd(age_fd); %change to folder for specific age range results
list_results = dir(age_fd);
num_results = length(list_results) - 2; %subtract parent folder & subfolder
(. & ..) to get number of PSD files

for i=3:length(list_results)  %start at 3 so you skip . & ..
    fname = list_results(i).name;
    load(fname);
%   Pre-feed
    if(exist('EGG_pre1_psd') && exist('EGG_pre2_psd'))
        EGG_pre = [EGG_pre1_psd EGG_pre2_psd];
        EGG_pre_avg = mean(EGG_pre,2);
    elseif(exist('EGG_pre1_psd'))
        EGG_pre_avg = EGG_pre1_psd;
    else
        EGG_pre_avg = EGG_pre2_psd;
    end
%   During-feed:
```

```
    if(exist('EGG_dur1_psd') && exist('EGG_dur2_psd'))
        EGG_dur = [EGG_dur1_psd EGG_dur2_psd];
        EGG_dur_avg = mean(EGG_dur,2);
    elseif(exist('EGG_dur1_psd'))
        EGG_dur_avg = EGG_dur1_psd;
    else
        EGG_dur_avg = EGG_dur2_psd;
    end
%   Post-feed:
    if(exist('EGG_post1_psd') && exist('EGG_post2_psd'))
        EGG_post = [EGG_post1_psd EGG_post2_psd];
        EGG_post_avg = mean(EGG_post,2);
    elseif(exist('EGG_post1_psd'))
        EGG_post_avg = EGG_post1_psd;
    else
        EGG_post_avg = EGG_post2_psd;
    end

    pwr_dur_pre(i-2,:) = EGG_dur_avg./EGG_pre_avg;
    pwr_post_pre(i-2,:) = EGG_post_avg./EGG_pre_avg;

end
clear EGG_pre1_psd EGG_dur1_psd EGG_post1_psd EGG_pre2_psd EGG_dur2_psd
EGG_post2_psd i EGG_dur1_psd
%% Average & calculate STE power ratio for each period

% Calculate power ratio average
pwr_dur_pre_avg(z,:) = mean(pwr_dur_pre);
pwr_post_pre_avg(z,:) = mean(pwr_post_pre);

if(z==1)
    pwr_dur_pre_early = pwr_dur_pre;
    pwr_post_pre_early = pwr_post_pre;
elseif(z==2)
    pwr_dur_pre_mid = pwr_dur_pre;
    pwr_post_pre_mid = pwr_post_pre;
else
    pwr_dur_pre_term = pwr_dur_pre;
    pwr_post_pre_term = pwr_post_pre;
end

pwr_dur_pre_STE(z,:) = std(pwr_dur_pre)/sqrt(num_results);
pwr_post_pre_STE(z,:) = std(pwr_post_pre)/sqrt(num_results);
pwr_dur_pre_STD(z,:) = std(pwr_dur_pre);
pwr_post_pre_STD(z,:) = std(pwr_post_pre);

mPSD_post_subs(:,1) = mean(pwr_post_pre(:,10:34),2);
mPSD_post_subs(:,2)= mean(pwr_post_pre(:,35:67),2);
mPSD_post_subs(:,3) = mean(pwr_post_pre(:,68:151),2);

% FOR ANOVA:

for i=3:length(list_results)  %start at 3 so you skip . & ..
    if(i==3)
        b_dur(:,:) = pwr_dur_pre(i-2,10:34)';
```

```
        n_dur(:,:) = pwr_dur_pre(i-2,35:67)';
        t_dur(:,:) = pwr_dur_pre(i-2,68:151)';

        b_post(:,:) = pwr_post_pre(i-2,10:34)';
        n_post(:,:) = pwr_post_pre(i-2,35:67)';
        t_post(:,:) = pwr_post_pre(i-2,68:151)';
    else
        b_dur = cat(1,b_dur,pwr_dur_pre(i-2,10:34)');
        n_dur = cat(1,n_dur,pwr_dur_pre(i-2,35:67)');
        t_dur = cat(1,t_dur,pwr_dur_pre(i-2,68:151)');

        b_post = cat(1,b_post,pwr_post_pre(i-2,10:34)');
        n_post = cat(1,n_post,pwr_post_pre(i-2,35:67)');
        t_post = cat(1,t_post,pwr_post_pre(i-2,68:151)');
    end
end
clear b_dur n_dur t_dur b_post n_post t_post;

mPSD_dur_b(z,:) = pwr_dur_pre_avg(z,10:34);
mPSD_dur_n(z,:) = pwr_dur_pre_avg(z,35:67);
mPSD_dur_t(z,:) = pwr_dur_pre_avg(z,68:151);

mPSD_post_b(z,:) = pwr_post_pre_avg(z,10:34);
mPSD_post_n(z,:) = pwr_post_pre_avg(z,35:67);
mPSD_post_t(z,:) = pwr_post_pre_avg(z,68:151);

clear mPSD_dur_subs mPSD_post_subs pwr_dur_pre pwr_post_pre;

end

%% t-tests
% Bradygastria
[h_b_dur_earlymid, p_b_dur_earlymid] =
ttest(mPSD_dur_b(1,:),mPSD_dur_b(2,:));
[h_b_dur_midterm, p_b_dur_midterm] = ttest(mPSD_dur_b(2,:),mPSD_dur_b(3,:));
[h_b_dur_earlyterm, p_b_dur_earlyterm] =
ttest(mPSD_dur_b(1,:),mPSD_dur_b(3,:));

[h_b_post_earlymid, p_b_post_earlymid] =
ttest(mPSD_post_b(1,:),mPSD_post_b(2,:));
[h_b_post_midterm, p_b_post_midterm] =
ttest(mPSD_post_b(2,:),mPSD_post_b(3,:));
[h_b_post_earlyterm, p_b_post_earlyterm] =
ttest(mPSD_post_b(1,:),mPSD_post_b(3,:));

% Normogastria
[h_n_dur_earlymid, p_n_dur_earlymid] =
ttest(mPSD_dur_n(1,:),mPSD_dur_n(2,:));
[h_n_dur_midterm, p_n_dur_midterm] = ttest(mPSD_dur_n(2,:),mPSD_dur_n(3,:));
[h_n_dur_earlyterm, p_n_dur_earlyterm] =
ttest(mPSD_dur_n(1,:),mPSD_dur_n(3,:));

[h_n_post_earlymid, p_n_post_earlymid] =
ttest(mPSD_post_n(1,:),mPSD_post_n(2,:));
```

```
[h_n_post_midterm, p_n_post_midterm] =
ttest(mPSD_post_n(2,:),mPSD_post_n(3,:));
[h_n_post_earlyterm, p_n_post_earlyterm] =
ttest(mPSD_post_n(1,:),mPSD_post_n(3,:));

% Tachygastria
[h_t_dur_earlymid, p_t_dur_earlymid] =
ttest(mPSD_dur_t(1,:),mPSD_dur_t(2,:));
[h_t_dur_midterm, p_t_dur_midterm] = ttest(mPSD_dur_t(2,:),mPSD_dur_t(3,:));
[h_t_dur_earlyterm, p_t_dur_earlyterm] =
ttest(mPSD_dur_t(1,:),mPSD_dur_t(3,:));

[h_t_post_earlymid, p_t_post_earlymid] =
ttest(mPSD_post_t(1,:),mPSD_post_t(2,:));
[h_t_post_midterm, p_t_post_midterm] =
ttest(mPSD_post_t(2,:),mPSD_post_t(3,:));
[h_t_post_earlyterm, p_t_post_earlyterm] =
ttest(mPSD_post_t(1,:),mPSD_post_t(3,:));




%% Plots for power ratio curve
cpm = freq_EGG_psd .* 60; %gastric spectrum: 0.5-9 cpm; 0.48 (9) - 9 (151)
(9-51)

% During/Pre
figure;
ax = axes();
for i=1:length(age_range)
e =
errorbar(ax,cpm(10:151,:),pwr_dur_pre_avg(i,10:151),pwr_dur_pre_STE(i,10:151)
);
if(i==1)
    e.Color = '#4DBEEE';
elseif(i==2)
    e.Color = "#D95319";
else
    e.Color = "#77AC30";
end
hold on;
end
set(ax, 'XScale', 'log');
xlabel('Frequency (cpm)'); ylabel('Power Ratio'); title('Power Ratio: During
/ Pre');
xticks([0.54 2.04 4.02 9.0]);
xticklabels({'0.5','2','4','9'}); xlim([0.5 9]);
ylim([0 3]); yticks([0:1:3]); yticklabels({'0','1','2','3'});
legend('Early','Mid','Term');
a = get(gca,'XTickLabel');
set(gca,'XTickLabel',a,'fontsize',12,'FontWeight','bold')
ax = gca;
ax.FontSize = 16;

% legend('DFI','PFI','NFI');
```

```
% Post/Pre:
figure;
ax = axes();
for i=1:length(age_range)
e =
errorbar(ax,cpm(10:151,:),pwr_post_pre_avg(i,10:151),pwr_post_pre_STE(i,10:15
1));
if(i==1)
    e.Color = '#4DBEEE';
elseif(i==2)
    e.Color = "#D95319";
else
    e.Color = "#77AC30";
end
hold on;
end
% for adults:
% load('adults_new.mat');
% e = errorbar(ax,cpm(10:151,:),mPR_avg(10:151),mPR_STE(10:151));
e.Color="#7E2F8E";


set(ax, 'XScale', 'log');
xlabel('Frequency (cpm)'); ylabel('Power Ratio'); title('Power Ratio: Post /
Pre');
xticks([0.54 2.04 4.02 9.0]);
xticklabels({'0.5','2','4','9'}); xlim([0.5 9]);
ylim([0 3]); yticks([0:1:3]); yticklabels({'0','1','2','3'});
% ylim([0 30]);
legend('Early','Mid','Term');
a = get(gca,'XTickLabel');
set(gca,'XTickLabel',a,'fontsize',12,'FontWeight','bold')
ax = gca;
ax.FontSize = 16;
% legend('DFI','PFI','NFI');



%% Mean Power Ratio

clear i;
% mPR_dur(age,freq band)
for i=1:length(age_range)
    mPR_dur(i,1) = mean(pwr_dur_pre_avg(i,10:34),2);
    mPR_dur(i,2) = mean(pwr_dur_pre_avg(i,35:67),2);
    mPR_dur(i,3) = mean(pwr_dur_pre_avg(i,68:151),2);

    mPR_post(i,1) = mean(pwr_post_pre_avg(i,10:34),2);
    mPR_post(i,2) = mean(pwr_post_pre_avg(i,35:67),2);
    mPR_post(i,3) = mean(pwr_post_pre_avg(i,68:151),2);

%     idk if these errors are correct
```

```
    if(i==1)%early
        mPR_dur_STE(i,1) =
std(pwr_dur_pre_early(:,10:34),0,"all")/sqrt(length(pwr_dur_pre_early(:,10:34
))); %brady
        mPR_dur_STE(i,2) =
std(pwr_dur_pre_early(:,35:67),0,"all")/sqrt(length(pwr_dur_pre_early(:,35:67
))); %normo
        mPR_dur_STE(i,3) =
std(pwr_dur_pre_early(:,68:151),0,"all")/sqrt(length(pwr_dur_pre_early(:,68:1
51))); %tachy

        mPR_post_STE(i,1) =
std(pwr_post_pre_early(:,10:34),0,"all")/sqrt(length(pwr_dur_pre_early(:,10:3
4))); %brady
        mPR_post_STE(i,2) =
std(pwr_post_pre_early(:,35:67),0,"all")/sqrt(length(pwr_dur_pre_early(:,35:6
7))); %normo
        mPR_post_STE(i,3) =
std(pwr_post_pre_early(:,68:151),0,"all")/sqrt(length(pwr_dur_pre_early(:,68:
151))); %tachy
    elseif(i==2) %mid
        mPR_dur_STE(i,1) =
std(pwr_dur_pre_mid(:,10:34),0,"all")/sqrt(size(pwr_dur_pre_mid,1)*length(pwr
_dur_pre_early(:,10:34))); %brady
        mPR_dur_STE(i,2) =
std(pwr_dur_pre_mid(:,35:67),0,"all")/sqrt(size(pwr_dur_pre_mid,1)*length(pwr
_dur_pre_early(:,35:67))); %normo
        mPR_dur_STE(i,3) =
std(pwr_dur_pre_mid(:,68:151),0,"all")/sqrt(size(pwr_dur_pre_mid,1)*length(pw
r_dur_pre_early(:,68:151))); %tachy

        mPR_post_STE(i,1) =
std(pwr_post_pre_mid(:,10:34),0,"all")/sqrt(size(pwr_post_pre_mid,1)*length(p
wr_dur_pre_early(:,10:34))); %brady
        mPR_post_STE(i,2) =
std(pwr_post_pre_mid(:,35:67),0,"all")/sqrt(size(pwr_post_pre_mid,1)*length(p
wr_dur_pre_early(:,35:67))); %normo
        mPR_post_STE(i,3) =
std(pwr_post_pre_mid(:,68:151),0,"all")/sqrt(size(pwr_post_pre_mid,1)*length(
pwr_dur_pre_early(:,68:151))); %tachy
    else
        mPR_dur_STE(i,1) =
std(pwr_dur_pre_term(:,10:34),0,"all")/sqrt(size(pwr_dur_pre_term,1)*length(p
wr_dur_pre_early(:,10:34))); %brady
        mPR_dur_STE(i,2) =
std(pwr_dur_pre_term(:,35:67),0,"all")/sqrt(size(pwr_dur_pre_term,1)*length(p
wr_dur_pre_early(:,35:67))); %normo
        mPR_dur_STE(i,3) =
std(pwr_dur_pre_term(:,68:151),0,"all")/sqrt(size(pwr_dur_pre_term,1)*length(
pwr_dur_pre_early(:,68:151))); %tachy

        mPR_post_STE(i,1) =
std(pwr_post_pre_term(:,10:34),0,"all")/sqrt(size(pwr_post_pre_term,1)*length
(pwr_dur_pre_early(:,10:34))); %brady
```

```
        mPR_post_STE(i,2) =
std(pwr_post_pre_term(:,35:67),0,"all")/sqrt(size(pwr_post_pre_term,1)*length
(pwr_dur_pre_early(:,35:67))); %normo
        mPR_post_STE(i,3) =
std(pwr_post_pre_term(:,68:151),0,"all")/sqrt(size(pwr_post_pre_term,1)*lengt
h(pwr_dur_pre_early(:,68:151))); %tachy
    end
end

%% Plot mPR (bar plot)
cpm = freq_EGG_psd .* 60; %gastric spectrum: 0.5-9 cpm; 0.48 (9) - 9 (151)
(9-51)
M = categorical({'Bradygastria','Normogastria','Tachygastria'});
M = reordercats(M,{'Bradygastria','Normogastria','Tachygastria'});


for j=1:2 %2 figures: 1 = during/pre & 2 = post/pre
figure;
if(j==1)
    brady = mPR_dur(:,1);
    normo = mPR_dur(:,2);
    tachy = mPR_dur(:,3);


%     brady_err = mPSD_dur_pre_STD(:,1,1);
%     normo_err = mPSD_dur_pre_STD(:,2,1);
%     tachy_err = mPSD_dur_pre_STD(:,3,1);
    brady_err = mPR_dur_STE(:,1,1);
    normo_err = mPR_dur_STE(:,2,1);
    tachy_err = mPR_dur_STE(:,3,1);


else
    brady = mPR_post(:,1);
    normo = mPR_post(:,2);
    tachy = mPR_post(:,3);

%     brady_err = mPSD_post_pre_STD(:,1,1);
%     normo_err = mPSD_post_pre_STD(:,2,1);
%     tachy_err = mPSD_post_pre_STD(:,3,1);

    brady_err = mPR_post_STE(:,1);
    normo_err = mPR_post_STE(:,2);
    tachy_err = mPR_post_STE(:,3);


    %     Adding adults:
%     brady(4) = 1.4997; normo(4) = 4.85; tachy(4) = 23.3759;
end

bands = [brady normo tachy]';
bands_err = [brady_err normo_err tachy_err]';
% for adults:
% if(j==2)
```

```
%     bands_err(4,:) = 0.0315;
% end

h = bar(M,bands);% h will have 3 handles, one for each color of bars

hBar = bar(bands, 0.8);                                                    %
Return 'bar' Handle
set(hBar(:,1),'FaceColor',"#4DBEEE"); set(hBar(:,2),'FaceColor',"#D95319");
set(hBar(:,3),'FaceColor',"#77AC30");
for k1 = 1:size(bands,2)
    ctr(k1,:) = bsxfun(@plus, hBar(k1).XData, hBar(k1).XOffset');       %
Note: 'XOffset' Is An Undocumented Feature, This Selects The 'bar' Centres
    ydt(k1,:) = hBar(k1).YData;                                            %
Individual Bar Heights
end
hold on
errorbar(ctr, ydt, bands_err, '.r')                                        %
Plot Error Bars
hold off
set(gca,'XTickLabel',M)
legend('Early','Mid','Term');
ylim([0 6]);
% legend('DFI','PFI','NFI');
a = get(gca,'XTickLabel');
set(gca,'XTickLabel',a,'fontsize',12,'FontWeight','bold')
ax = gca;
ax.FontSize = 16;

ylabel('Power Ratio');
% ylim([0 3.5]);
% yticks([-0.5:0.5:3.5]); %yticklabels({'0' '1' '2' '3' '4' '5'});
if(j==1)
    title("During/Pre Mean Power Ratio");
else
    title("Post/Pre Mean Power Ratio");
end
end
```

PMA Analysis for mPR (PSDvsPMA_new.m):

```
% Makes scatter plot of mPR vs. PMA (separate for pre/dur/post &
brady/normo/tachy)
clear all; close all;
pma_fd = 'F:\Fall 2022 EGG PSD Practice\All PSD Data\PMA analysis';
cd(pma_fd);

weeks = dir(pma_fd);
week_num = length(weeks) - 2; %-2 to remove . & ..

%% Average PSD for each week
%i for week, j for subject
```

```
for i=3:length(weeks) %for week
    wk = weeks(i).name;
    wk_fd = [pma_fd,'\',wk];
    cd([pma_fd,'\',wk]);
    list_results = dir(wk_fd);
    num_results = length(list_results) - 2;
    num_results_all(i-2,:) = num_results;
    for j=3:length(list_results)    %average for all subjects within a week
        fname = list_results(j).name;
        load(fname);
        if(exist('EGG_pre1_psd') && length(EGG_pre1_psd)==250001 &&
exist('EGG_pre2_psd') && length(EGG_pre2_psd)==250001)
            EGG_pre = [EGG_pre1_psd EGG_pre2_psd];
            EGG_pre = mean(EGG_pre,2);
        elseif(exist('EGG_pre1_psd') && length(EGG_pre1_psd)==250001)
            EGG_pre = EGG_pre1_psd;
        elseif(exist('EGG_pre2_psd') && length(EGG_pre2_psd)==250001)
            EGG_pre = EGG_pre2_psd;
        end

        if(exist('EGG_dur1_psd') && length(EGG_dur1_psd)==250001 &&
exist('EGG_dur2_psd') && length(EGG_dur2_psd)==250001)
            EGG_dur = [EGG_dur1_psd EGG_dur2_psd];
            EGG_dur = mean(EGG_dur,2);
        elseif(exist('EGG_dur1_psd') && length(EGG_dur1_psd)==250001)
            EGG_dur = EGG_dur1_psd;
        elseif(exist('EGG_dur2_psd') && length(EGG_dur2_psd)==250001)
            EGG_dur = EGG_dur2_psd;
        end

        if(exist('EGG_post1_psd') && length(EGG_post1_psd)==250001 &&
exist('EGG_post2_psd') && length(EGG_post2_psd)==250001)
            EGG_post = [EGG_post1_psd EGG_post2_psd];
            EGG_post = mean(EGG_post,2);
        elseif(exist('EGG_post1_psd') && length(EGG_post1_psd)==250001)
            EGG_post = EGG_post1_psd;
        elseif(exist('EGG_post2_psd') && length(EGG_post2_psd)==250001)
            EGG_post = EGG_post2_psd;
        end

        EGG_dur_pre(j-2,:) = EGG_dur./EGG_pre;
        EGG_post_pre(j-2,:) = EGG_post./EGG_pre;

        clear EGG_pre1_psd EGG_dur1_psd EGG_post1_psd EGG_pre2_psd
EGG_dur2_psd EGG_post2_psd;
    end
%   EGG_dur_pre and EGG_post_pre contain the power ratio curves for each
subject.

%   Calculate mean power ratio by bands
    mPR_dur_brady(i-2,:) = mean(mean(EGG_dur_pre(:,10:34),2));
mPR_dur_brady_STE(i-2,:) =
std(mean(EGG_dur_pre(:,10:34),2))/sqrt(num_results);
    mPR_dur_normo(i-2,:) = mean(mean(EGG_dur_pre(:,35:67),2));
mPR_dur_normo_STE(i-2,:) =
std(mean(EGG_dur_pre(:,35:67),2))/sqrt(num_results);
```

```
    mPR_dur_tachy(i-2,:) = mean(mean(EGG_dur_pre(:,68:151),2));
mPR_dur_tachy_STE(i-2,:) =
std(mean(EGG_dur_pre(:,68:151),2))/sqrt(num_results);

    mPR_post_brady(i-2,:) = mean(mean(EGG_post_pre(:,10:34),2));
mPR_post_brady_STE(i-2,:) =
std(mean(EGG_post_pre(:,10:34),2))/sqrt(num_results);
    mPR_post_normo(i-2,:) = mean(mean(EGG_post_pre(:,35:67),2));
mPR_post_normo_STE(i-2,:) =
std(mean(EGG_post_pre(:,35:67),2))/sqrt(num_results);
    mPR_post_tachy(i-2,:) = mean(mean(EGG_post_pre(:,68:151),2));
mPR_post_tachy_STE(i-2,:) =
std(mean(EGG_post_pre(:,68:151),2))/sqrt(num_results);


    clear EGG_dur_pre EGG_post_pre EGG_pre EGG_dur EGG_post;
end


%% Plot mean power ratio
week_list = 24:40;
dx = 0.1; dy = 0.1; % displacement so the text does not overlay the data
points
n = num2str(num_results_all); n = cellstr(n);
n1 = n(1:13); n2 = n(14:17);
for k=1:2 %1 = dur, 2 = post
    if(k==1) %dur/pre
        dy=0.01;
        figure; %bradygastria
        scatter(week_list,mPR_dur_brady,'filled','LineWidth',1);
        errorbar(week_list,mPR_dur_brady,mPR_dur_brady_STE,'LineWidth',1);

text(week_list(1:13),mPR_dur_brady(1:13)+mPR_dur_brady_STE(1:13)+dy,n1);
        text(week_list(14:17),mPR_dur_brady(14:17)-mPR_dur_brady_STE(14:17)-
dy,n2);
        title('During/Pre-Feeding: Bradygastria');
        xlabel('Post-Menstrual Age (Weeks)');
        ylabel('Power Ratio');
        xlim([23.5 40.5]);
        ylim([0 5]);
        a = get(gca,'XTickLabel');
set(gca,'XTickLabel',a,'fontsize',12,'FontWeight','bold')
%         xticks([24:1:40]);
% ax = gca;
% ax.FontSize = 16;

        figure; %normogastria
        scatter(week_list,mPR_dur_normo,'filled','LineWidth',1);
        errorbar(week_list,mPR_dur_normo,mPR_dur_normo_STE,'LineWidth',1);

text(week_list(1:13),mPR_dur_normo(1:13)+mPR_dur_normo_STE(1:13)+dy,n1);
        text(week_list(14:17),mPR_dur_normo(14:17)-mPR_dur_normo_STE(14:17)-
dy,n2);
        title('During/Pre-Feeding: Normogastria');
        xlabel('Post-Menstrual Age (Weeks)');
        ylabel('Power Ratio');
```

```
        xlim([23.5 40.5]);
        ylim([0 5]);
        a = get(gca,'XTickLabel');
set(gca,'XTickLabel',a,'fontsize',12,'FontWeight','bold')
% ax = gca;
% ax.FontSize = 16;

        figure; %tachygastria
        scatter(week_list,mPR_dur_tachy,'filled','LineWidth',1);
        errorbar(week_list,mPR_dur_tachy,mPR_dur_tachy_STE,'LineWidth',1);

text(week_list(1:13),mPR_dur_tachy(1:13)+mPR_dur_tachy_STE(1:13)+dy,n1);
        text(week_list(14:17),mPR_dur_tachy(14:17)-mPR_dur_tachy_STE(14:17)-
dy,n2);
        title('During/Pre-Feeding: Tachygastria');
        xlabel('Post-Menstrual Age (Weeks)');
        ylabel('Power Ratio');
        xlim([23.5 40.5]);
        ylim([0 5]);

        a = get(gca,'XTickLabel');
set(gca,'XTickLabel',a,'fontsize',12,'FontWeight','bold')
% ax = gca;
% ax.FontSize = 16;
    end
    if(k==2) %Post/Pre
        dy=0.1;
        figure; %bradygastria
        scatter(week_list,mPR_post_brady,'filled','LineWidth',1);
        errorbar(week_list,mPR_post_brady,mPR_post_brady_STE,'LineWidth',1);

text(week_list(1:13),mPR_post_brady(1:13)+mPR_post_brady_STE(1:13)+dy,n1);
        text(week_list(14:17),mPR_post_brady(14:17)-
mPR_post_brady_STE(14:17)-dy,n2);
        title('Post/Pre-feeding: Bradygastria');
        xlabel('Post-Menstrual Age (Weeks)');
        ylabel('Power Ratio');
        ylim([0 3.5]);
%         scale = -0.5:0.5:4.5;
%         yticks(scale);
        xlim([23.5 40.5]);
        a = get(gca,'XTickLabel');
set(gca,'XTickLabel',a,'fontsize',12,'FontWeight','bold')
% ax = gca;
% ax.FontSize = 16;

        figure; %normogastria
        scatter(week_list,mPR_post_normo,'filled','LineWidth',1);
        errorbar(week_list,mPR_post_normo,mPR_post_normo_STE,'LineWidth',1);

text(week_list(1:13),mPR_post_normo(1:13)+mPR_post_normo_STE(1:13)+dy,n1);
        text(week_list(14:17),mPR_post_normo(14:17)-
mPR_post_normo_STE(14:17)-dy,n2);
        title('Post/Pre-feeding: Normogastria');
        xlabel('Post-Menstrual Age (Weeks)');
        ylabel('Power Ratio');
```

```
        ylim([0 3.5]);
%         scale = -0.5:0.5:4.5;
%         yticks(scale);
        xlim([23.5 40.5]);
        a = get(gca,'XTickLabel');
set(gca,'XTickLabel',a,'fontsize',12,'FontWeight','bold')
% ax = gca;
% ax.FontSize = 16;

        figure; %tachygastria
        scatter(week_list,mPR_post_tachy,'filled','LineWidth',1);
        errorbar(week_list,mPR_post_tachy,mPR_post_tachy_STE,'LineWidth',1);

text(week_list(1:13),mPR_post_tachy(1:13)+mPR_post_tachy_STE(1:13)+dy,n1);
        text(week_list(14:17),mPR_post_tachy(14:17)-
mPR_post_tachy_STE(14:17)-dy,n2);
        title('Post/Pre-feeding: Tachygastria');
        xlabel('Post-Menstrual Age (Weeks)');
        ylabel('Power Ratio');
        ylim([0 3.5]);
%         scale = -0.5:0.5:4.5;
%         yticks(scale);
        xlim([23.5 40.5]);
        a = get(gca,'XTickLabel');
set(gca,'XTickLabel',a,'fontsize',12,'FontWeight','bold')
% ax = gca;
% ax.FontSize = 16;
    end

end
```